Optimization of accelerator and brake in photosynthetic electron transport

Leonardo Basso

Table of Contents

LIST OF ABBREVIATIONS

AL: Actinic Light

AMS: 4-Acetamido-4-isothiocyanato-2,2-stilbenedisulfonic acid disodium salt hydrate

CET: Cyclic electron transport

CPA: Cation/proton antiporter 2

CRR2: CHLORORESPIRATORY REDUCTION 2

C-terminal: carboxyl-terminal

Cyt: Cytochrome

DPGR: DISTURBED PROTON GRADIENT REGULATION

ECS: Electrochromic shift

ETR: Electron transport rate

Fd: Ferredoxin

Flv: Flavodiiron proteins

g_{H^+}: H^+ conductivity of thylakoid ATP synthase

HL: High light

KEA: K^+ efflux antiporter

KTN: K^+ transport/nucleotide-binding

LET: Linear electron transport

LL: Low light

min: minute

NADPH: reduced nicotinamide adenine dinucleotide phosphate

$NADP^+$: oxidized nicotinamide adenine dinucleotide phosphate

NDH: NADH dehydrogenase-like complex

nm: nanometre

NPQ: non-photochemical quenching

N-terminal: amino-terminal

PAGE: polyacrylamide gel electrophoresis

PAM: Pulse amplitude modulation

PFD: photon flux density

PPFD: Photosynthetic photon flux density

PGR5: PROTON GRADIENT REGULATION 5

PGRL1: PRG5-LIKE PHOTOSYNTHETIC PHENOTYPE 1

pmf: proton motive force

PS: photosystem

$P700^+$: oxidized PSI reaction center

PPR: pentatricopeptide repeat

PQ: plastoquinone

PVDF: polyvinylidene difluoride

qE: energization-dependent excitation quenching

ROS: Reactive oxygen species

s: second

SD: Second

SDS: sodium dodecyl sulfate

SE: Standard error

WT: wild type

Y(II): Photosystem II yield

Y(I): Photosystem I yield

ΔpH: proton gradient across the thylakoid membrane

Δψ: membrane potential across the thylakoid membrane

ABSTRACT

In photosynthesis, light-dependent electron transport generates an electrochemical gradient of protons contributing to proton motive force (pmf) across the thylakoid membrane. The pmf is used to drive the ATP synthesis by CF_o-CF_1-ATP synthase. Formation of pmf also downregulates photosynthetic electron transport by the regulation of the cytochrome (Cyt) b_6f complex activity and the dissipation of excessively absorbed light energy from photosystem II (PSII) antennae. These two opposite functions are regulated by the two components of pmf: the membrane potential ($\Delta\psi$) and the proton concentration gradient (ΔpH). To optimize the photosynthetic performance to the fluctuating light environments, the size and partitioning of two components ($\Delta\psi$ and ΔpH) should be precisely regulated by a series of regulatory systems. In this work, I tried to clarify the collaboration of regulatory machineries and to artificially optimize the trade-off between the accelerator (ATP synthesis) and the brake (downregulation of electron transport).

In Chapter 1, I focused on the contribution of KEA3 and NDH-dependent cyclic electron transport (CET) around photosystem I (PSI) to efficiently initiate photosynthesis after long dark adaptation. A series of mutants were used to monitor the induction of photosynthesis. The Arabidopsis *kea3-1* mutant is defective in the putative H^+/K^+ antiporter localized to the thylakoid membrane. KEA3 functions in the rapid relaxation of ΔpH-dependent downregulation by substituting ΔpH by $\Delta\psi$. The *chlororespiratory reduction 2-1* (*crr2-1*) mutation is defective in CET depending on the chloroplast NADH dehydrogenase-like (NDH) complex. After the overnight dark adaptation, relaxation of transiently induced NPQ was delayed in the *kea3-1* mutant. Unexpectedly, the *crr2-1* mutation enhanced this phenotype in the *kea3-1* mutant background. KEA3 is important to initiate photosynthesis efficiently by relaxing large ΔpH and the NDH complex assists the process probably via its reverse reaction rather than the canonical CET activity. By carefully analysing the induction of photosynthesis, we propose a collaborative model of KEA3 and NDH contributing to the flexible induction of photosynthesis. In the double mutant, induction of CO_2 fixation was delayed, suggesting the physiological significance of this regulatory network.

In Chapter 2, the double transgenic line overexpressing KEA3 and Flavodiiron (Flv) proteins originated from *Physcomitrella patens* was generated and characterized. In the KEA3ox line, contribution of $\Delta\psi$ to pmf was high, resulting in the reduced extent of brake at the Cyt b_6f complex. A problem is the overflow of electrons toward PSI, leading to the photodamage of PSI. This risk was avoided by the introduction of Flv, which absorbed

excessively accumulating electrons from PSI. The double transgenic line behaved ideally under the fluctuating light intensity. Immediately after the shift from low light to high light, Flv kept PSI oxidized, protecting PSI from photodamage. On the contrary, after shift from high light to low light, energy dissipation from PSII was immediately relaxed in the double transgenic line. This is beneficial for plants to keep the high level of CO_2 fixation under the fluctuating light intensity. I will discuss the possibility on the artificial optimization of the accelerator and brake in photosynthetic electron transport.

GENERAL INTRODUCTION

Photosynthesis consists of two sets of reactions. In the light ones, absorption of photons activates electron transport via two photosystems (PS) in the thylakoid membrane. In linear electron transport (LET), photosystem II (PSII) catalyzes the light-dependent oxidation of H_2O, resulting in the release of O_2 and protons (H^+) into the thylakoid lumen (Fig. 1). Electrons released from water are transferred from PSII to PSI, and ultimately to $NADP^+$ which receives electrons from ferredoxin (Fd), resulting in the generation of NADPH. The cytochrome (Cyt) b_6f complex mediates the electron transport between two photosystems by driving plastoquinone (PQ)-dependent plastocyanin (PC) reduction. Coupled with this electron transport, the Cyt b_6f complex translocated H^+ from the stroma to the thylakoid lumen by the quinone (Q) cycle, contributing to the generation of a proton concentration gradient across the thylakoid membrane (ΔpH). Together with the membrane potential (Δψ) formed across the thylakoid membrane, ΔpH forms the proton motive force (pmf) (Fig. 2). The pmf is used by F_0F_1-ATP synthase in chloroplasts to produce ATP (Kramer et al., 2003; Soga et al., 2017).

The chemical energy stored in the light reactions (ATP and NADPH) is used by the second set of reactions, the Calvin-Benson-Bassham (CBB) cycle to fix atmospheric CO_2 to sugars. The CBB cycle requires an ATP/NADPH at the ratio of 1.5 in the absence of oxygenase reaction of Rubisco, but the ratio achieved solely by LET is approximately 1.29 (Allen, 2002). To satisfy the ATP/NADPH production ratio, additional electron transport is necessary. Cyclic electron transport around PSI (CET), recycles electrons from the acceptor side of PSI (Fd) to the PQ pool through two possible pathways (Fig. 1). CET does not generate reducing equivalents or O_2 but contributes to the formation of ΔpH. In angiosperms, CET consists of two pathways depending on PROTON GRADIENT REGULATION 5 (PGR5) and the NADH dehydrogenase-like (NDH) complex (Munekage et al., 2002; Munekage et al., 2004; DalCorso et al., 2008). In *Arabidopsis thaliana* (Arabidopsis), the antimycin A-sensitive, PGR5-dependent pathway is the main route for CET and contributes to the generation of pmf across the thylakoid membrane, resulting in ATP synthesis (Munekage et al., 2002; DalCorso et al., 2008; Wang et al., 2015). The NADH dehydrogenase-like (NDH) complex-dependent pathway is insensitive to antimycin A (Munekage et al., 2004). The NDH complex pumps four protons, coupled with the movement of two electrons, from two molecules of Fd to PQ, further increasing the efficiency of ΔpH formation (Strand et al., 2017).

The pmf is used to drive the energy production by ATP synthase and to induce the mechanisms that downregulates photosynthesis under excessive light conditions. Although both ΔpH and Δψ contribute to ATP synthesis as components of pmf, only the ΔpH is responsible for the

downregulation of photosynthetic electron transport by acidifying the thylakoid lumen (Shikanai et al., 2016) (Fig. 2). In particular, ΔpH-dependent lumenal acidification downregulates the photosynthetic electron transport at the Cyt b_6f complex, the process that is called photosynthetic control and is a very important mechanism to protect PSI especially under fluctuating light conditions. Lumenal acidification also downregulates the efficiency of light energy utilization in PSII (Stiehl and Witt, 1969 and Müller et al., 2001). The latter dissipates the excess of energy absorbed by PSII antennae as heat and this regulatory process is monitored as an energization-dependent (qE) component of non-photochemical quenching (NPQ) of chlorophyll fluorescence (Miller et al., 2002).

CET is the main regulatory mechanism for the size of pmf. In contrast, partitioning of the two pmf components (ΔpH and Δψ) is regulated by channels or transporters embedded in the thylakoid membrane (Spetea et al.,2017 and Carrarretto et al., 2013). K^+ exchange antiporter 3 (KEA3) belongs to the CPA2 (cation/proton antiporter2) and recently gained attention because of its ability of regulating the partitioning of pmf components. In addition to KEA3 localized to the thylakoid membrane (Armbruster et al., 2014; Wang et al., 2017), KEA1 and KEA2 are present in the chloroplast envelope and collaborate with KEA3 for the ion homeostasis in the chloroplast (Ferro et al., 2010; Simm et al., 2013). KEA3 has been proposed to efflux H^+ from the thylakoid lumen and import K^+ as a counter ion (Maser et al., 2001) but it has not been experimentally demonstrated (Tsujii et al., 2019).

Regulation of pmf plays a key role in the optimization of the trade-off between the efficient utilization of light energy and photoprotection. Absorption of excessive light energy is harmful for plants and thus they have developed some systems to dissipate the excess of energy to avoid damages caused by production of reactive oxygen species (ROS). Chlorophylls become excited by absorbing photons. Excited chlorophylls return to their basal state through four processes: 1) transferring energy to neighbouring chlorophylls, 2) emitting fluorescence, 3) charge separation or 4) thermal energy dissipation. If the processes are inefficient, reaction centre chlorophylls (P680) may transfer the energy to O_2, leading to the generation of singlet oxygen (Asada et al., 1999). The induction of qE is the process to avoid the generation of ROS by thermal energy dissipation.

In the field, intensity of light fluctuates rapidly and dynamically. It is difficult for plants to adapt to this inconstant condition consisting of the transition between low light (LL) and high light (HL) phases. In the LL phase, the downregulation is not induced and the rate of electron transport (ETR) is maximized between two photosystems. Immediately after transition from LL to HL, plants have to induce the downregulation of electron transport to avoid photodamage. Especially, the downregulation at the Cyt b_6f complex plays a crucial role to avoid the photodamage of PSI (Suorsa et al., 2012). Because the Arabidopsis *pgr5* mutant cannot induce this photosynthetic control, the mutant is sensitive to the fluctuating light intensity (Tikkanen et

al., 2010). On the opposite transition, from HL to LL, plants have to relax the downregulation as quick as possible or light intensity would strongly limits the rate of photosynthesis in the early LL phase.

Photodamage of PSI is caused by the trap of electrons in PSI (Yamori et al., 2016). To avoid this PSI photodamage, photosynthetic control plays an essential role (Suorsa et al., 2013). Additionally, plants have developed mechanisms to pump out electrons from PSI. At the acceptor side of PSI, excess electrons are often used for O_2 reduction via the Mehler reaction (Asada, 2000). Resulting superoxide is dissipated by superoxide dismutase (SOD) and ascorbate peroxidase (APX). As far as ROS is efficiently detoxified, this water–water cycle dissipates the excess of energy by consuming the reducing equivalents produced by PSI and also by regenerating ascorbate via the Asada cycle (Asada, 2000). In addition to scavenging ROS, the water-water cycle may regulate the ATP/NADPH production ratio by mediating pseudoCET. However, the rate of O_2 reduction depending on the Mehler reaction is not high in angiosperms (Badger et al., 2000; Shirao et al., 2013). Much more efficient O_2 reduction at the acceptor side of PSI depends on Flavodiiron proteins (Flv), a family of enzymes that catalyse O_2 or NO reduction to H_2O and N_2O (Allahverdiyeva et al., 2015). A flavin mononucleotide moiety of Flv likely accepts electrons from NADPH or Fd, while a lactamase-like domain containing a non-heme diiron center is involved in O_2 reduction. In divergent phototrophs from cyanobacteria to gymnosperms, the Flv1/Flv3-type heterodimer protects PSI from photodamage especially under fluctuating light intensity (Allahverdiyeva et al., 2013). Despite their high conservation in phototrophs, angiosperms have lost Flv (Allahverdiyeva et al., 2015). Some studies (Yamamoto et al., 2016 Yamamoto et al., 2019) showed how the introduction of exogenous Flv could recover the severe photodamage of PSI in the *pgr5* plants under fluctuating light conditions. Flv is an excellent safety valve in the electron transport and the reason why angiosperms lost them is unclear.

Both ΔpH and $\Delta\psi$ contribute to the ATP synthesis as components of pmf, but only the ΔpH downregulates electron transport. It may be possible to regulate accelerator and brake independently by artificially controlling the ratio of ΔpH and $\Delta\psi$. A systemic biological approach may also clarify how pmf is optimized for two conflicting demands of generating ATP (accelerator) and dissipating the excess energy (brake). By modifying the activity of CET, channels or transporters, it may be possible to change the size of pmf and the ratio of ΔpH and $\Delta\psi$. The modification of the component ratio is the most straightforward strategy because we may generate plants able to use as much of the absorbed light energy for photoreactions, optimizing photosynthesis. The key point should be the discovery of the best balance between the accelerator and brake. Flv may be able to support this artificial modification of photosynthesis by moving the balance to the more positive side as an excellent safety valve.

The goal of my Ph.D. studies was to clarify the crosstalk among proteins in the regulation of pmf. In particular, I focused on the regulation of pmf by the collaboration of the NDH complex and KEA3 in Arabidopsis (Chapter 1). In the second part, I took a systemic biological approach by focusing on the regulation of the photosynthesis in the Arabidopsis transgenic line that overexpresses KEA3 and Flv originated from *Physchomitrella patens* (Chapter 2). Finally, I will discuss how the artificial reoptimization of pmf is effective for improving the productivity of plants.

CHAPTER 1: Collaboration between NDH and KEA3 allows maximally efficient photosynthesis after a long dark adaptation

1.1 INTRODUCTION

In the light reactions of photosynthesis, the absorption of photons activates two photosystems, resulting in the activation of two types of electron transport. In LET, PSII catalyses the light-dependent oxidation of H_2O, leading to the release of O_2 and protons into the thylakoid lumen. Excised electrons from water are transferred to PSI through the Cyt b_6f complex and ultimately to $NADP^+$, producing NADPH. This electron transport is coupled with the translocation of H^+ from the stroma to the thylakoid lumen via the Q cycle at the Cyt b_6f complex, resulting in the formation of a proton concentration gradient across the thylakoid membrane. This ΔpH contributes to the formation of pmf, in addition to the membrane potential formed across the thylakoid membrane (Δψ) that results from the uneven distribution of ions across the membrane. The pmf energizes ATP synthesis via F_0F_1-ATP synthase in chloroplasts (Kramer et al., 2003; Soga et al., 2017) and thus influences the efficiency of photosynthesis.

The CBB cycle depends on NADPH and ATP produced by the light reactions. To fix a molecule of CO_2 into a carbohydrate, three molecules of ATP and two molecules of NADPH are needed. However, this ratio of ATP/NADPH (1.5) is not satisfied by LET (Shikanai et al., 2007). Photorespiration, which takes place via oxygenation of RuBP due to the low specificity of Rubisco to CO_2 increases the energetic requirements in terms of ATP, raising the ATP/NADPH ratio up to 1.67. The additional ATP is thought to be supplied by CET (Yamori and Shikanai, 2016). In contrast to LET, CET is driven solely by PSI and does not contribute to the net production of reducing power. CET recycles electrons from Fd to the PQ pool and contributes to the additional generation of ΔpH via the Q cycle. As a result, CET balances the production ratio of ATP and NADPH. In angiosperms, CET has been proposed to consist of two pathways; the PROTON GRADIENT REGULATION 5 (PGR5)/PGR5-like Photosynthetic Phenotype 1 (PGRL1) protein-dependent, antimycin A-sensitive pathway and the NDH complex-dependent antimycin A-insensitive pathway (Munekage et al., 2004). The NDH complex is considered to pump four protons, coupled with the movement of two electrons from Fd to PQ, further increasing the efficiency of ΔpH formation (Strand et al., 2017).

In addition to ATP synthesis, the ΔpH component of pmf also contributes to the downregulation of electron transport (Shikanai, 2014). Acidification of the thylakoid lumen triggers the thermal dissipation of excessively absorbed light energy from the PSII antennae, a process that is monitored by NPQ of chlorophyll fluorescence (Müller et al., 2001). Low lumenal pH also downregulates the activity of the Cyt b_6f complex, slowing down the rate of electron transport toward PSI (Stiehl and Witt, 1969). CET-dependent ΔpH formation is also necessary to induce the downregulation of electron transport, as indicated by the phenotype of the *pgr5* mutant. The *Arabidopsis*

thaliana (Arabidopsis) *pgr5* mutant cannot induce thermal dissipation under excessive light conditions (Munekage et al., 2002), suggesting that CET-dependent ΔpH plays an important role in sufficiently acidifying the thylakoid lumen to trigger NPQ induction. The *pgr5* mutant is also defective in the downregulation of Cyt b_6f activity, resulting in hypersensitivity of PSI to the fluctuating light intensity (Tikkanen et al., 2010; Yamamoto et al., 2016). Compared to the physiological function of the PGR5/PGRL1-dependent CET, the contribution of the NDH-dependent CET to photoprotection is somewhat minor, although clear phenotypes have been observed in the mutants defective in NDH at LL intensity and also under fluctuating light intensity (Ueda et al., 2012; Yamori et al., 2015; Yamori et al., 2016). The physiological function of the NDH complex has not been fully clarified.

Both ΔpH and Δψ contribute to pmf, but only ΔpH downregulates electron transport. To optimize the operation of the accelerator (ATP synthesis) and the brake on electron transport, it is necessary to precisely regulate the ratio of the two pmf components, as well as the total size of pmf (Cruz et al., 2001; Kramer et al., 2003). Several channels and antiporters localized to the thylakoid membrane regulate the partitioning of the pmf components (Spetea et al., 2017). K^+ efflux antiporter 3 (KEA3) is thought to be a H^+/K^+ antiporter localized to the thylakoid membrane (Armbruster et al., 2014; Kunz et al., 2014), although its antiport activity has not been experimentally demonstrated (Tsujii et al., 2019). Based on its structure, topology and the mutant phenotypes, KEA3 most likely moves H^+ from the thylakoid lumen while taking up K^+ as a counter ion. Consequently, KEA3 transforms ΔpH to Δψ and is necessary to rapidly relax the downregulation of electron transport by raising the lumenal pH. The C-terminal domain of KEA3, KTN (K^+ transport/nucleotide binding) is exposed to the stroma (Wang et al., 2017) and is thought to downregulate its activity by monitoring ATP or NADPH levels (Schlosser et al., 1993; Roosild et al., 2002). However, information on the regulation of KEA3 is limited. Armbruster et al. (2014) demonstrated that KEA3 contributes to efficient photosynthesis under fluctuating light conditions. The *disturbed proton gradient regulation* (*dpgr*) is a dominant mutant allele of *KEA3* and its mutant phenotype is evident after a long period of dark adaptation (overnight) (Wang et al., 2017). KEA3 is likely important during the induction of photosynthesis, as well as under fluctuating light intensities. The similarity between the two conditions suggests that KEA3 is required for readjusting the ΔpH-dependent regulation immediately after any drastic change in light conditions.

In this study, I characterized the double mutants defective in the CET pathways and KEA3 to understand whether and how the synergy between CET and KEA3 affects the regulatory network of photosynthesis. Especially, I focused on the contribution of NDH-dependent CET during the induction of photosynthesis after overnight dark adaptation in the *kea3-1* mutant context. Based on our results, I propose a novel physiological function of the NDH

complex, which would allow greater flexibility of the regulatory network during the induction of photosynthesis.

1.2 MATERIALS AND METHODS

1.2.1 Plant Materials and Growth Conditions

Arabidopsis thaliana Wild Type, (ecotype Columbia gl1), mutant plants and transgenic plants overexpressing PGR5 were grown in soil in a growth chamber (50–60 μmol photons $m^{-2}s^{-1}$) under long-day conditions (16-h light/8-h dark cycles, 23˚C) for 3 to 4 weeks. Fully expanded leaves were used for experiments. The mutants and transgenic lines used in this study are *kea3-1* (GABI_170G09, Wang et al., 2017), *pgr5-1* (previously called pgr5, Munekage et al., 2002), *crr2-1* (Hashimoto et al., 2003), *crr2-1kea3-1* (Wang et al., 2017) *pnsb2/ndf2* (Salk_111363, Takabayashi et al., 2009) *kea3-1pnsb2/ndf2* (Basso et al., 2020) 35Sp::PGR5 #2 and 35Sp::PGR5 #2 *crr2-1*(Okegawa et al., 2007).

1.2.2 Analysis of Chlorophyll Fluorescence

Chlorophyll fluorescence and P700 absorption changes in the PSI reaction center were measured simultaneously using a portable chlorophyll fluorometer (DUAL-PAM-100 MODULAR version chlorophyll fluorescence and P700 absorption analyzer equipped with a p700 dual-wavelength emitter at 830 and 870 nm; Walz). Plants were kept in the dark for 30 min or 8 h before the measurements. Detached leaves were used for the analysis. Minimal fluorescence in the dark-adapted state (F0) was excited by a weak measuring light (620 nm) at a photon flux density of 0.05 to 0.1 μmol photons m^{-2} s^{-1}. A saturating pulse of light (SP; 300 ms, 10,000 μmol photons m^{-2} s^{-1}) was applied to determine the maximal fluorescence in the dark-adapted state (Fm) and during actinic light (AL) illumination (Fm'). The steady-state fluorescence level (Fs) was recorded during AL illumination (110 μmol photons m^{-2} s^{-1}) just before the supply of an SP. The maximum quantum yields of PSII and NPQ were calculated as Fv/Fm and (Fm-Fm')/Fm', respectively. Y(II) was calculated as (Fm-Fs)/Fm'.

The redox change of P700 was assessed by monitoring the changes in absorbance of transmission light at 830 nm and 875 nm. Pm was determined by the application of an SP in the presence of far-red light (720 nm). The maximal level of oxidized P700 during AL illumination (Pm') was determined by an SP application. The steady-state P700 level (P) was recorded just before the supply of an SP. Y(I) was calculated as (Pm' – P)/Pm. Y(NA) was calculated as (Pm – Pm')/Pm. Y(ND) was calculated as P/Pm. Three complementary quantum yields were defined as Y(I) + Y(NA) + Y(ND) = 1 (Klughammer and Schreiber, 1994). The relative level of reduced P700 was calculated as 1 – Y(ND). The value can vary between 0 (P700 fully oxidized) and 1 (P700 fully reduced) in a given state.

1.2.3 ECS measurements

The ECS measurements were carried out using a Dual-PAM 100 equipped with a P515/535 module (Walz). Measurements were carried out in ambient air. Before the measurements, 4–5 week-old plants grown under a short-day photoperiod were dark-adapted for overnight, followed by 10-min illumination with 110 µmol photons m^{-2} s^{-1} actinic red light (> 8h). A 1-s dark pulse was applied at the different time points to record the ECSt level, which represents the size of the light-induced pmf and was estimated from the total amplitude of the rapid decay of the ECS signal during the dark pulse, as described previously (Wang et al., 2015). ECSt levels were normalized against a 515-nm absorbance change induced by a single turnover flash (ECS_{ST}), as measured in dark-adapted leaves before recording. This normalization makes it possible to take into account possible changes in leaf thickness and chloroplast density between leaves (Takizawa et al., 2008).

1.2.4 Gas Exchange

The gas exchange rate was measured using a gas-exchange cuvette (GFS 3000, Walz) equipped with a Dual Pam Cuvette (DUAL 3010 cuvette, Walz) with an illuminated area of 1.3 cm^2 and 1 mm chamber depth. Leaf temperature was kept close to 23˚C (22.5–23.5˚C). Incoming CO_2 and H_2O concentrations were controlled via the GFS-3000 Gas Exchange System. The gas stream (400 µmol s^{-1}) passed the leaf twice, over the lower and upper sides, before entering the Infrared Gas Analyzer for assessment of CO_2 uptake and H_2O release at a PPFD of 100 µmol photons m^{-2} s^{-1} under adjusted air conditions (400 ppm CO_2, 21% O_2). The rate of mitochondrial respiration in the light was assumed to be equal to that in the dark. The gross rate of CO_2 assimilation was calculated as the sum of the net CO_2 assimilation rate and dark respiration rate. Measurements were performed on individual 4-week-old seedlings that had been kept in the dark for 30 min or 8 h before the analysis.

1.2.5 SDS-PAGE and Immunoblot Analyses

Plants were frozen in liquid nitrogen after dark adaptation or after a different light treatment and disrupted using a Shake master (Shake Master Neo, bms). Proteins were extracted in SDS sample buffer [2% (w/v) sodium dodecyl sulfate (SDS), 62.5 mM Tris-HCl (pH 6.8), 7.5% (v/v) glycerol, 6M urea] containing the protease inhibitor cocktail Complete (Roche, Mannheim, Germany) and the specific thiol-labeling reagent AMS (Invitrogen, Carlsbad, CA, USA). The samples were incubated for 60 min at room temperature to complete the labeling of thiol groups with AMS. Protein concentration was determined via a BCA protein assay (Pierce, Rockford, IL, USA). Proteins were separated by non-reducing SDS polyacrylamide gel electrophoresis (PAGE) using the conventional Laemmli (Tris–glycine) system (Laemmli, 1970) and transferred onto polyvinylidene fluoride (PVDF) membranes using

a semi-dry blotting apparatus. Immunodetection was carried out using specific antibodies. Signals were detected using an ECL Plus Western Blotting Detection Kit (GE Healthcare) and visualized by a LAS300 chemiluminescence analyzer (Fuji Film; http://www.fujifilm.com). Immunoblots were quantified by Imagemaster software (Amersham Pharmacia Biotech).

1.2.6 Statistical Analyses

Statistical analyses were performed using the Tukey-Kramer test and the Dunnett test.

1.3 RESULTS

1.3.1 The *kea3-1 pgr5-1* Double Mutant Combines the Phenotypes of the Single Mutants in NPQ Induction

To study the collaboration between KEA3 and CET during the induction of photosynthesis, we characterized a series of Arabidopsis mutants. The *pgr5* mutant is defective in the main pathway of CET (Munekage et al., 2002). In this study, we used the original strong allele of *pgr5*, which is referred to as *pgr5-1* in recent studies (Yamamoto et al., 2019; Nakano et al., 2019) to distinguish from the weak allele of *pgr5-2*. The *kea3-1* mutant is a knockout allele of *KEA3* that encodes a putative H^+/K^+ transporter (Ferro et al., 2010; Armbruster et al., 2014; Kunz et al., 2014). The H^+ efflux activity is important in regulating the lumenal pH and consequently in inducing the rapid relaxation of the energy-dependent quenching (qE) of NPQ. In the mutant, the ablation of this pathway leads to a higher NPQ level and a delay in its relaxation (Armbruster et al., 2014).

In this study, we analyzed the *kea3-1 pgr5-1* double mutant. The plants were adapted to the dark overnight (>8 h) before the analysis of electron transport. The CBB cycle enzymes are inactivated during this long dark adaptation (Buchanan, 2016). In the *kea3-1* mutant, the relaxation of NPQ was significantly delayed during the induction of photosynthesis by relatively LL (110 µmol photons m^{-2} s^{-1}) after the overnight dark adaptation, in accordance with our previous data (Wang et al., 2017) (Fig. 1-1A). Since the induction of the CBB cycle is delayed to a higher extent after overnight dark adaptation, the contribution of KEA3 to the relaxation of NPQ is higher than after 30-min dark adaptation.

In WT plants, NPQ was transiently induced to the maximum level within 1 min after the onset of AL (Fig. 1-1A). In the *pgr5-1* mutant, however, AL did not induce this transient peak of NPQ, and the low level of NPQ was not relaxed for 5 min (Table 1A). Consistent with previous reports (Armbruster et al., 2014; Wang et al., 2017), the *kea3-1* mutant displayed a slightly higher maximum NPQ level and a delay in the relaxation of NPQ compared to WT plants (Fig. 1-1A). The *kea3-1 pgr5-1* double mutant did not induce a transient peak in NPQ but the NPQ level was higher than that of the *pgr5-1* mutant 1–4 min after the onset of AL, and it was higher than that of the *kea3-1* mutant 3 min after the onset of AL (Fig. 1-1A). This phenotype recorded in the double mutants is consistent with the fact that the *pgr5-1* mutant and the *kea3-1* mutant are respectively defective in pmf formation and relaxation of ΔpH. We also monitored the induction of LET by a Y(II) parameter representing the quantum yield of PSII after overnight dark adaptation (Fig. 1-1B). In the *pgr5-1* mutant background, the induction of LET

was delayed (Table 1-1A) but Y(II) was close to the WT level after 5 min. The *kea3-1* mutation did not affect Y(II) in either the WT or *pgr5-1* mutant contexts.

1.3.2 The *crr2-1* Mutation Boosts the High NPQ Phenotype of the *kea3-1* Mutant during Induction of Photosynthesis after Overnight Dark Adaptation

Subsequently, we analyzed the collaboration of KEA3 with another pathway of PSI CET depending on the chloroplast NDH complex (Peltier et al., 2016). The *crr2-1* mutant is defective in the expression of the *ndhB* gene in chloroplasts and consequently lacks NDH activity (Hashimoto et al., 2003). In contrast to the *pgr5-1* mutant, the *crr2-1* mutation induced transient NPQ but its peak and relaxation were slightly delayed after overnight dark adaptation (Fig. 1-1C). The relaxation of NPQ was again more significantly delayed in the *kea3-1* mutant, as confirmed by the Dunnett test (Table 1B). Unexpectedly, the induction of NPQ was synergistically enhanced in the *crr2-1 kea3-1* double mutant (Table 1B). This is in contrast to the combined, intermediate phenotype of the *pgr5-1 kea3-1* double mutant (Fig. 1-1A). Interestingly, it took longer for transient NPQ to peak in the *crr2-1 kea3-1* double mutant (100–120 s after the onset of AL) than in the WT (40 s after the onset of AL).

In the *crr2-1* and *kea3-1* single mutants, LET monitored by Y(II) was only mildly affected during the induction of photosynthesis after overnight dark adaptation. However, the induction of LET was delayed in the *crr2-1 kea3-1* double mutant (Fig. 1-1D, Table 1B). Taken together with the observations of NPQ induction and relaxation (Fig. 1-1C), our interpretation is that the thylakoid lumen may have been more acidified in the *crr2-1 kea3-1* double mutant than in the single mutants. This hypothesis is consistent with the idea that the *kea3-1* mutant context accumulates more protons in the lumen, but it is unclear how the defect in the NDH complex enhances the *kea3-1* phenotype. We therefore focused on this phenotype of the double mutant to analyze the collaboration between KEA3 and NDH.

To assess the impact of the long overnight dark adaptation on the *crr2-1 kea3-1* mutant phenotype, we analyzed the induction of photosynthesis at the same photosynthetic photon flux density (PPFD) (110 μmol photons m^{-2} s^{-1}) after a 30-min dark adaptation (Fig. 1-2). This short dark adaptation is routinely used before chlorophyll fluorescence analysis to relax pmf formed under growth lighting. Both single mutants (*crr2-1* and *kea3-1*) showed similar induction and relaxation curves of NPQ to those after overnight dark adaptation (Figs. 1-1C and 1-2A). However, NPQ was not further affected in the *crr2-1 kea3-1* double mutant and was similar to that of the *kea3-1* single mutant (Table 2). Thus, the overnight dark adaptation enhanced the phenotype of the *crr2-1 kea3-1* mutant. A similar trend was also observed in Y(II), although the induction of LET was also delayed in the *crr2-1 kea3-1*

double mutant with respect to other genotypes after 30-min dark adaptation (Fig. 1-2B, Table 2).

The *crr2-1* mutant is defective in a pentatricopeptide repeat (PPR) protein required for the expression of the plastid *ndhB* gene (Hashimoto et al., 2003). The *crr2-1* mutation might also affect the expression of other plastid gene(s) and the phenotype of the *crr2-1 kea3-1* double mutant might be caused by the altered expression of the unknown gene(s) rather than *ndhB*. To eliminate this possibility, we also created the double mutant of *kea3-1* with the *photosynthetic ndh subunit 2 of subcomplex b* (*pnsb2*) mutant directly defective in the nuclear gene encoding a subunit of the NDH complex (Ifuku et al., 2011). As with the *crr2-1* mutation, the *pnsb2* mutation enhanced the mutant phenotype of *kea3-1* in NPQ and Y(II), although the difference was not statistically significant by the Tukey-Kramer test (Fig. 1-3, A and B, Table 3). We confirmed that the defects in the accumulation of the NDH complex enhanced the *kea3-1* mutant phenotype after overnight dark adaptation.

1.3.4 Collaboration of the NDH Complex with KEA3 Is Necessary to Efficiently Induce LET

By monitoring the change in absorbance of the PSI reaction center chlorophylls (P700), we analysed the status of PSI photochemistry during the induction of photosynthesis at 110 μmol photons m^{-2} s^{-1}. Y(I) is often used to estimate the quantum yield of PSI and is calculated from a ratio of P700 in a reduced state but it is not limited by the acceptor side (P700 functioning in electron transport). The Y(ND) parameter is calculated as the ratio of oxidized P700 ($P700^+$) per total P700 and represents the non-photochemical energy dissipation from oxidized PSI. Y(ND) is used to estimate the operation of the ΔpH-dependent downregulation of the Cyt b_6f complex (photosynthetic control), which is important to control the rate of electron transport toward PSI (Yamamoto and Shikanai, 2019). In contrast, Y(NA) represents the fraction of reduced P700 that cannot be oxidized by a saturation pulse due to the lack of acceptors (non-photochemical energy dissipation from reduced PSI). In addition to the actual shortage of electron acceptors from PSI, Y(NA) is induced when excess electrons accumulate on the donor side of PSI (Klughammer and Schreiber, 1994). The induction of Y(NA) is related to the photodamage of PSI and inevitably occurs during the very early induction of photosynthesis and also just after the shift from LL to HL, even in WT plants (Yamamoto et al., 2016). Because light energy absorbed by the PSI antennae is photochemically used or non-photochemically dissipated via one of three processes, the sum of Y(I), Y(ND) and Y(NA) is 1.

After 30-min dark adaptation, no difference was observed in PSI photochemistry among WT, *crr2-1*, *kea3-1* and *crr2-1 kea3-1* plants (Fig. 1-4). Y(ND) was transiently induced during the early induction of the CBB cycle but was immediately substituted by Y(I). The time course of the induction

and relaxation of Y(ND) was similar to those of NPQ (Fig. 1-2), suggesting a transient acidification of the thylakoid lumen. Y(NA) was only induced during the initial phase (<40 s) but was immediately relaxed by the induction of Y(I) and (ND).

After overnight dark adaptation, the induction of Y(I) and Y(ND) were slightly delayed in the *crr2-1* mutant compared to the WT (Fig. 1-5, A and B, Table 4). The Y(ND) peaked at 60 s after the onset of AL in WT plants, but it peaked at 80–100 s in the *crr2-1* mutant (Fig. 1-5B). Consequently, it took longer to relax Y(NA) (Fig. 1-5C). The contribution of Y(ND) was slightly higher in the *kea3-1* mutant than in the WT during the subsequent relaxation and steady-state phases. The *kea3-1* mutant behaved almost like the *crr2-1* mutant. In the *crr2-1 kea3-1* double mutants, however, the *crr2-1* phenotypes were amplified (Fig. 1-5). Induction of Y(I) and Y(ND) was significantly delayed. The peak of Y(ND) was observed at 140–160 s after the onset of AL, resulting in the delay in the relaxation of Y(NA). During the relaxation and steady-state phases, the level of Y(ND) was higher than that in the other genotypes, resulting in a lower Y(I) level (Fig. 1-5B). This phenotype is consistent with the higher maximum level of NPQ and its delay in relaxation and the reduced level of Y(II) in the *crr2-1 kea3-1* double mutant (Fig. 1-1, C and D). During the relaxation and steady-state phases (>1 min after the onset of AL in WT plants), the thylakoid lumen was likely more acidified in the *crr2-1 kea3-1* double mutant than in other genotypes. Taken together with the results of chlorophyll fluorescence analyses (Fig. 1-1, C and D), we propose that the NDH complex likely contributes to the rapid acidification of the thylakoid lumen during the initial phase of photosynthetic induction (<60 s after the onset of AL) after overnight dark adaptation. On the other hand, the collaboration of the NDH complex with KEA3 is required for relaxing the ΔpH in the next relaxation phase (60–180 s after the onset of AL). This phase is important to efficiently induce photosynthesis, as can be deduced by the delayed induction of Y(II) and Y(I) (LET) in the *crr2-1 kea3-1* double mutants. A similar trend was observed in the *kea3-1 pnsb2* double mutant (Fig. 1-3, C, D and E).

To confirm our hypothesis that NDH contributes to the initial lumenal acidification, we performed electro-chromic shift (ECS) experiments. The ECS signal represents the changes in the absorption of photosynthetic pigments (mainly carotenoids) peaking at 515–520 nm, in the presence of an electric field across the thylakoid membrane (Klughammer et al., 2013). To characterize the phenotype of the *crr2-1 kea3-1* double mutant more comprehensively, we analyzed the ECS signal during the induction of photosynthesis at 110 μmol photons m^{-2} s^{-1} (Fig. 1-6). The total amplitude of ECS changes (ECSt) from a dark pulse during AL illumination (110 μmol photons m^{-2} s^{-1}) represents the total size of pmf formed in the light (Bailleul et al., 2010). The ECSt level was standardized by the ECS signal triggered with a single turnover flash (ECS_{ST}) to compensate for the effects of the differences in leaf thickness and the content of reaction centers. In the WT plants, the

size of pmf peaked at 40 s after the onset of AL after both conditions of dark adaptation and was followed by relaxation (Fig. 1-6, A and C). This is consistent with the course of induction and relaxation of NPQ and Y(ND) in the WT plants (Figs. 1-1C and 1-5B). For 1 min after the onset of AL, the size of pmf was smaller in the *crr2-1 kea3-1* double mutant than that of other genotypes after overnight dark adaptation (Fig. 6A, Table 5). This is consistent with the slower induction of Y(ND) seen in the double mutant (Fig. 5B) and suggests that the NDH-dependent CET is probably important to induce a transient increase in ΔpH in the initial phase (<60 s). The size of pmf did not show any peaks during the induction of photosynthesis in the *crr2-1 kea3-1* double mutants, and the level was similar to that of the other genotypes at 2 min after the onset of AL (Fig. 1- 6A). The size of pmf does not simply explain the delayed peak and relaxation of NPQ and Y(ND) in the *crr2-1 kea3-1* double mutant (Figs. 1-1C and 1-4B). It is necessary to consider relative partitioning, i.e., the higher contribution of ΔpH to pmf in the double mutant.

The g_{H^+} parameter, which is considered to represent the proton conductivity of ATP synthase (Kramer et al., 2004; Kohzuma et al., 2013), was determined by chasing the initial fast relaxation kinetics of the ECS in the dark. The g_{H^+} was drastically reduced in the *crr2-1 kea3-1* double mutant after overnight dark adaptation (Fig. 1-6B, Table 5), suggesting a delay in the activation of ATP synthase. After the 30-min dark adaptation, the reduction in g_{H^+} was milder in the *crr2-1 kea3-1* double mutant and similar to that in the *kea3-1* mutant, although a mild reduction was observed also in the *crr2-1* mutant context (Fig. 1-6D, Table 5).

The thioredoxin-dependent redox modification of the γ subunit of ATP synthase regulates the activity of ATP synthase during the induction of photosynthesis. The reduced form of the γ subunit was modified with 4-acetoamido-4-maleimidylstilbene-2,2-disulfonate (AMS) and was separated from the oxidized form by non-reducing SDS-PAGE (Motohashi et al., 2001). Immediately after the onset of AL (30 s), the γ subunit was reduced to the steady-state level and no difference was observed in the reduction state of the γ subunit between the WT and the *crr2-1 kea3-1* mutant after 30-min or overnight dark adaptation (Fig. 1-7). Thus, the activation of the γ subunit does not explain the lower g_{H^+} in the *crr2-1 kea3-1* double mutant.

1.3.5 The Contribution of KEA3 is Negligible to Induce Photosynthesis Efficiently under HL after Overnight Dark Adaptation

For studying the photosynthetic induction after overnight dark adaptation, we selected a relatively low PPFD of 110 μmol photons m^{-2} s^{-1} because the phenotype of the *kea3-1* mutant was most clearly observed at this PPFD (Wang et al., 2017). We also tested the induction of electron transport at a higher PPFD (300 μmol photons m^{-2} s^{-1}) after overnight dark adaptation (Fig. 1-8). Compared to the induction at 110 μmol photons m^{-2} s^{-1}, a higher level of NPQ was induced and was not relaxed for 280 s in the light in WT and *kea3-*

1 plants (Fig. 1-8A). The induction of NPQ was slightly delayed in the *crr2-1* mutant, the phenotype that was enhanced in the *crr2-1 kea3-1* double mutant. At 3 min after the onset of AL, the levels of NPQ became similar among all the genotypes. Induction of Y(II) was mildly affected in the *crr2-1* mutant background before 120 s and in the *kea3-1* mutant background after 120 s (Fig. 1-8B). Induction of Y(I) was more significantly delayed than Y(II) in the *crr2-1* mutant background (*crr2-1* and *crr2-1 kea3-1*) at 80 s after the onset of AL but Y(I) was restored to the WT level at 120 s (Fig. 1-8C, Table 6). This delay in Y(I) may reflect the lack of the NDH-dependent CET since Y(II) was only mildly affected in the *crr2-1* mutant background. The delay in the NPQ induction may be explained by the absence of NDH-dependent CET (Fig. 1-8, A, B and C). Consistent with this idea, the induction of Y(ND) was severely delayed at 80 s after the onset of AL in the *crr2-1* mutant background. This was reflected by the delay in the relaxation of Y(NA) at the same time (Fig. 1-8, D and E, Table 6). Notably, similar phenotypes were observed between the *crr2-1* mutant and the *crr2-1 kea3-1* double mutant, contrasting to the synergistic effect observed at 110 μmol photons m^{-2} s^{-1} (Figs. 1-1, 1-4 and 1-8). The function of KEA3 and also probably the reverse action of NDH are likely necessary only at a relatively LL intensity, where the ΔpH-dependent downregulation is immediately relaxed. At a higher PPFD of 300 μmol photons m^{-2} s^{-1}, however, the ΔpH-dependent downregulation is not relaxed once it is induced.

The mutant phenotypes were not observed after the 30-min dark adaptation (Fig. 1-2). Subsequently, we analyzed how long dark adaptation is necessary for monitoring the contribution of NDH and KEA3 during the induction of photosynthesis at 110 μmol photons m^{-2} s^{-1} (Fig. 1-9). As the representative mutant phenotypes of the *crr2-1 kea3-1* double mutant, we selected high NPQ and Y(ND) and low Y(II) levels at 2 min after the onset of AL after overnight dark adaptation (Figs. 1-1, C and D, and 1-4B). After a 1-h dark adaptation, the *crr2-1 kea3-1* mutant did not show any phenotypes, as after a 30-min dark adaptation (Figs. 1-2 and 1-9). However, a similar phenotype to the overnight dark adaptation was detected after a 2–3-h dark adaptation. At least 2-h dark adaptation is necessary to induce the state, in which the collaboration of the NDH complex and KEA3 is necessary to induce photosynthesis efficiently.

1.3.6 The *crr2-1* Mutation also Enhanced the Phenotypes of the *35Sp::PGR5* Line

As shown above, the *crr2-1* mutation boosted the phenotypes due to the high ΔpH in the *kea3-1* mutant, especially after the overnight dark adaptation (Figs. 1-1, 1-4 and 1-6). We tested the impact of the *crr2-1* mutation in another genetic context that exhibited a high ΔpH phenotype (Fig. 10). The expressing the *35Sp::PGR5* transgene accumulates high levels of the PGR5 protein and conditionally activates the PGR5-dependent CET when the stroma is highly

reduced, as it is during the induction of photosynthesis (Okegawa et al., 2007). We therefore generated a line with the transgene inserted into the same genome position in the *crr2-1* mutant background by crossing the *PGR5* over-expressing line with the *crr2-1* mutant (*35Sp::PGR5 crr2-1*). As in the *kea3-1* mutant, the maximum level of transient NPQ was enhanced and its relaxation was delayed in the *35Sp::PGR5* line after overnight dark adaptation (Fig. 1-10A, Table 7). As in the *kea3-1* mutant background, the phenotype of the *35Sp::PGR5* line in NPQ was enhanced by adding the *crr2-1* mutation. A similar trend was observed in the Y(ND) parameter (Fig. 1-11, Table 7), suggesting stronger acidification of the thylakoid lumen. Consistent with this idea, the induction of LET was delayed in the *35Sp::PGR5* line and was further slowed in the *35Sp::PGR5 crr2-1* line (Fig. 1-11, B and C, Table 7). In the same way with the *kea3-1* mutant background, the NDH complex is necessary to relax the transiently formed high ΔpH in the *35Sp::PGR5* backgrounds. The NDH complex engages with KEA3 to rapidly relax the transiently induced high ΔpH, a process that is necessary to efficiently induce LET after overnight dark adaptation.

1.3.7 Collaboration of the NDH Complex with KEA3 to Induce Efficient CO_2 Fixation after Overnight Dark Adaptation

The collaboration of the NDH complex with KEA3 is necessary to efficiently induce LET, as evaluated by the chlorophyll fluorescence and spectroscopic analyses (Figs. 1-1 and 1-4). Finally, we analyzed the impact of the *crr2-1* and *kea3-1* mutations and the *crr2-1 kea3-1* double mutation on the induction of CO_2 fixation at 110 μmol photons m^{-2} s^{-1} by GFS3000 (Walz) (Fig. 1-12), a system for the assessment of plant photosynthesis (CO_2-uptake) or respiration (CO_2-release) and transpiration. Simultaneously, we monitored the induction of Y(I) and Y(II) by the Dual-PAM system (Fig. 1-13). After 30-min dark adaptation, the rate of CO_2 fixation was not affected in any of the genetic backgrounds (Fig. 1-11B, Table 8). Consistently, the induction of Y(I) and Y(II) was unaffected although it was slightly delayed at 20 s after the onset of AL in the *crr2-1 kea3-1* double mutant (Fig. 1-13, B and D). In contrast, the induction of CO_2 fixation was more evidently delayed in the *crr2-1 kea3-1* double mutant after overnight dark adaptation (Fig. 1-12A, Table 8). A similar phenotype was also observed in the induction of Y(I) and Y(II) (Fig. 1-13, A and C). We conclude that the collaboration of the NDH complex with KEA3 is needed to induce photosynthesis efficiently after the overnight dark adaptation.

1.4 DISCUSSION

The ΔpH-dependent regulation of electron transport optimizes photosynthesis, especially under fluctuating light conditions. To regulate the lumenal pH, it is necessary to adjust the size and the component partitioning of pmf (Cruz et al., 2001). In angiosperms, CET plays a central role in the regulation of pmf size (Munekage et al., 2002; Munekage et al., 2004; DalCorso et al., 2008; Wang et al., 2015; Yamamoto et al., 2016). The PGR5/PGRL1-dependent CET is essential to induce ΔpH-dependent regulation; the qE, monitored by NPQ, and the donor-side regulation of PSI at the Cyt b_6f complex monitored by Y(ND) (Munekage et al., 2004; Suorsa et al., 2012). On the other hand, channels and transporters localized to the thylakoid membrane regulate the partitioning of pmf components (Kramer et al., 2003; Spetea et al., 2017). The putative H^+/K^+ antiporter KEA3 was discovered only recently, and little is known about it, especially regarding the regulation of its activity (Armbruster et al., 2014; Kunz et al., 2014; Wang et al., 2017). Furthermore, the link between the two regulatory systems, CET and the modulation of trans-thylakoid ion movement remains unclear. In the Arabidopsis *pgr5-1* mutant, the lack of CET results in a reduced size of pmf (Munekage et al., 2002; Wang et al., 2017). The size of pmf was complemented to the WT level by the introduction of *Physcomitrella patens* genes encoding Flavodiiron (Flv) proteins into the Arabidopsis *pgr5-1* mutant (Yamamoto et al., 2016). Flv reduces O_2 to H_2O at the acceptor side of PSI (Allahverdiyeva et al., 2015) and the Flv-dependent pseudoCET (water-water cycle) contributes to pmf formation in place of the PGR5-dependent CET. Despite the increased size of pmf, the contribution of Δψ to pmf was greater in the *pgr5-1* mutant plants accumulating Flv, resulting in the reduced size of NPQ at moderate light intensities (Yamamoto et al., 2016). This observation suggests crosstalk between PGR5-dependent CET and the regulation of trans-thylakoid ion movement to optimize the size and partitioning of pmf, although the exact molecular mechanism is unclear.

In the present study, we analyzed the collaboration between two CET pathways and KEA3. Similarly, to the *pgr5-1* mutant, the *kea3-1 pgr5-1* double mutant did not induce transient NPQ but induced higher NPQ 1–5 min after the onset of AL than the *pgr5-1* mutant (Fig. 1-1A). Both phenotypes are consistent with those of the single mutants. On the other hand, the *crr2-1* and *pnsb2* mutations synergistically enhanced the high NPQ phenotype of the *kea3-1* mutant (Fig. 1C and Fig. 1-3A). The NDH complex is part of the CET machinery, which contributes to pmf formation, so it was not expected that, when defective, it would enhance the high NPQ phenotype of the *kea3-1* mutant. To explain the phenotypes of the *crr2-1* single mutant and the *crr2-1 kea3-1* double mutant after overnight dark adaptation (Fig. 1-1, C and D), we may consider two distinct modes of action (Fig. 1-14D) of the NDH complex based on the following considerations.

1) During the initial phase of photosynthetic induction (<60 s), the peak in transient NPQ was delayed in the *crr2-1* mutant (Fig. 1-1C). A similar delay was observed in the induction of Y(ND) (Fig. 1-4B). During this phase, the NDH complex may work in the canonical way to protonate the thylakoid lumen to support the induction of the mechanism of photoprotection. NDH activity might be counterbalanced by the proton efflux activity of KEA3 (Fig. 1-14 A, D). It thus seems likely that the NDH-dependent CET is necessary, as well as the PGR5-dependent CET, to efficiently induce the transient NPQ.

2) In the subsequent phase for the relaxation of NPQ (1–5 min after the onset of AL), the NPQ induction was more enhanced in the *crr2-1 kea3-1* double mutant than in the WT and the single mutants (Fig. 1-1C). Because this phenotype was not evident in the *crr2-1* single mutant, the NDH complex is dispensable when KEA3 is functional (Fig.1-14 B). The *kea3-1* mutant exhibited the high NPQ phenotype to a lower extent in this phase as well, suggesting that substitution of ΔpH by Δψ is necessary for rapidly relaxing NPQ. The higher NPQ induction in the double mutant cannot be explained by the canonical proton pumping activity of the NDH complex, where electrons are moved from Fd to PQ (Stand et al., 2017). We have to consider a novel activity of the NDH complex (Fig. 1-14D). In the absence of KEA3 and during the induction of photosynthesis, the lumenal pmf is likely to be high, as a consequence, a strong photosynthetic control is induced (Fig. 1-1D). Therefore, the electrons accumulate in the PQ pool. If this condition occurs in the presence of the NDH complex, it may mediate the transfer of electrons from the PQ pool to Fd. The passage of electrons against redox potential from PQ to Fd requires energy, which may be supplied by coupling with the reverse movement protons from the thylakoid lumen to the stroma supported by pmf. This reaction might be important to avoid the possible PSII damages by alleviating the overreduction of the PQ pool by directly oxidising the PQ pool and also by relaxing too large ΔpH. Although direct evidences are still lacking, uncouplers enhanced the NDH-dependent PQ reduction, suggesting that the back pressure of pmf controls NDH activity and may induce a reverse reaction (Stand et al., 2017). The uphill reaction of complex I (PQ-dependent Fd reduction) was also reported in bacteria, including *Rhodobacter capsulatus* (Heter et al., 1997) and *Thiobacillus ferrooxidans* (Elbehti et al., 2000) and was recently suggested in cyanobacteria (Nikkanen et al., 2020). This hypothesis is exciting because if the reverse reaction is confirmed, it may give an explanation for the loss of Flv in the angiosperms, besides from deepening our knowledge of the NDH complex.

The two modes of NDH activity were also supported by the analysis of P700 (Fig. 1-4). Induction of Y(ND) was delayed in the *crr2-1* single mutant and more severely in the *crr2-1 kea3-1* double mutant (Fig. 1-4B). The delay in the induction of Y(ND) resulted in the delay in the relaxation of Y(NA). Of interest is that induction of Y(II) and Y(I) was similarly delayed at 40–60 s after the onset of AL (Figs. 1-1D and 1-4A). This delay in the LET induction may be due to the acceptor limitation from PSI (Fig. 1-4C), but it is unclear

how the synergy between the NDH complex and KEA3 is necessary in the initial phase. To conclude the reverse reaction of the NDH complex, direct biochemical evidence would be necessary. We do not eliminate the possibility that lack of NDH-dependent CET secondarily disturbs the movement of protons from the thylakoid membrane.

In the second phase for relaxing NPQ, namely 1–5 min after the onset of AL, a high level of Y(ND) was induced in the *crr2-1 kea3-1* double mutant, supporting the idea that the thylakoid lumen was unusually acidified. This is probably the reason for the further delay in LET observed in Y(II) and Y(I) (Figs. 1-1D and 1-4A). In this phase, we speculate that the reverse reaction of the NDH complex takes place to optimize the lumenal pH. Disturbance of electron transport regulation in both phases likely resulted in the delay observed in the induction of CO_2 fixation (Fig. 1-12A). The reduced size of g_{H^+} in the *crr2-1 kea3-1* double mutant is consistent with the delay in the induction of CO_2 fixation (Fig. 1-6B) but was not due to the delay in the reduction of the γ subunit of ATP synthase (Fig. 1-7).

It is even more challenging to explain the molecular basis of the double mutant phenotypes in the initial phase (<60 s after the onset of AL). The total size of pmf peaked 40–60 s after the onset of AL in the WT and the *crr2-1* and *kea3-1* single mutants (Fig. 1-6A), consistent with the peaks of NPQ and Y(ND) in these genotypes (Figs. 1-1C and 1-4B). Puzzlingly, the size of pmf did not fluctuate and was consistently low during the induction of photosynthesis in the *crr2-1 kea3-1* double mutant (Fig. 1-6A). To explain the delayed induction and relaxation of NPQ and Y(ND), we need to consider the greater contribution of Δψ to pmf in the initial phase and the more significant contribution of ΔpH to pmf in the second phase. It is not feasible to analyze the partitioning of the pmf components during the induction of photosynthesis because the ECS signal is still unstable. Although we do not understand the mechanism, KEA3 was also required for transiently induce the high pmf during the initial phase (Fig. 1-6A). Although the *crr2-1* and *kea3-1* single mutants induced similar levels of transient pmf within 40 s after the onset of AL, Y(ND) induction was affected only in the *crr2-1* mutant (Fig. 1-3B). Because KEA3 is a putative H^+/K^+ antiporter, it would be logical to consider a higher contribution of ΔpH to pmf in the *kea3-1* mutant context. On the other hand, induction of Y(ND) was delayed at 40 s after the onset of AL in the *crr2-1* single mutant, as well as the *crr2-1 kea3-1* double mutant (Fig. 1-4B), although the level of pmf in the *crr2-1* mutant was between the levels of the WT and the *crr2-1 kea3-1* mutant (Fig. 1-4A). The phenotype may be explained by the threshold of ΔpH required for the induction of Y(ND). It is also possible that the NDH complex may be necessary to induce a transiently higher contribution of ΔpH to pmf in the initial phase.

In contrast to the induction by relatively low PPFD (110 μmol photons m^{-2} s^{-1}), the *kea3-1* mutation did not enhance the *crr2-1* phenotype at 300 μmol photons m^{-2} s^{-1} after overnight dark adaptation (Fig. 1-8). The lack of the NDH-dependent CET resulted in the delayed induction of Y(I), subsequently

delaying the induction of ΔpH-dependent downregulation of electron transport monitored in NPQ and Y(ND). The contribution of the NDH-dependent CET after long dark adaptation has been also suggested in the other study (Nikkanen et al., 2018). This function of NDH is likely the same as that in the initial phase of photosynthetic induction (<60 s) observed at 110 μmol photons m^{-2} s^{-1}. The impact of the *kea3-1* mutation in the *crr2-1* mutant background was not observed at 300 μmol photons m^{-2} s^{-1}. In the subsequent phase (1–5 min after the onset of AL), there was no difference anymore in photosynthetic parameters between WT and any of the mutants at 300 μmol photons m^{-2} s^{-1} (Fig. 1-8). This is consistent with the fact that the contribution of KEA3 is not observed at HL intensities (Wang and Shikanai, 2019). The second phase is probably specifically observed at a relatively LL intensity, at which the transiently induced ΔpH-dependent downregulation is relaxed. In the process, the collaboration of KEA3 and probably the reverse reaction of the NDH complex is necessary.

In conclusion, in this study, we focused on the mutant phenotype observed after overnight dark adaptation. The phenotype was suppressed after 30 min of dark adaptation (Figs. 1-2 and 1-6, C and D). Collaboration between the NDH complex and KEA3 is needed to efficiently induce photosynthesis in the initial phase at relatively LL intensity after overnight dark adaptation. This may be related to ion homeostasis in the stroma to activate the CBB cycle (Bloom and Lancaster, 2018). Further work is necessary to understand how exactly the two types of machinery interact. However, the idea of regulation of a H^+-conducting complex by an ion channel/transporter in the thylakoids is more than plausible, considering observations that a calcium-dependent potassium channel has been shown to functionally interact with complex IV of the respiratory chain (Bednarczyk et al., 2013) while complex II is regulated by an ATP-dependent potassium channel (Wojtovich et al., 2013).

CHAPTER 2: Remodelling of the photosynthetic electron transport by the Thylakoid H^+/K^+ Antiporter KEA3 and flavodiiron proteins in Arabidopsis.

2.1 INTRODUCTION

In chloroplasts, light energy absorbed by photosynthetic pigments associated with two photosystems drives electron transport from water to $NADP^+$. In this LET, the synthesis of NADPH is coupled with the proton translocation across the thylakoid membrane by the water splitting in PSII and the Q cycle by the Cyt b_6f complex. In addition to LET, CET recycles electrons from the acceptor side of PSI to the Cyt b_6f complex. PGR5 and PGRL1 proteins are necessary for the antimycin A-sensitive, main route of electron flow. The NDH complex also mediates the minor and regulatory pathway of CET, as described in the previous chapter.

In addition to CET, O_2 reduction at the acceptor side of PSI also mediates the alternative pathway of electron transport, mediating electron transport from water used for water splitting to water generated by O_2 reduction (Asada, 1999). This water-water cycle is also called pseudoCET and contributes to the generation of ΔpH, like CET. In angiosperms, this O_2 reduction depends on the Mehler reaction and approximately 1% of electrons derived from PSII are used for this pseudoCET (Shirao et al., 2013). The Mehler reaction is unlikely to be a large safety valve of electrons from PSI. The different type of water-water cycle depending on Flv was discovered in cyanobacteria (Helman et al., 2003). Flv directly reduces O_2 to water by accepting two electrons from NADPH or Fds (Vicente et al., 2002). In cyanobacteria, up to 20% of electrons derived from PSII are used for O_2 reduction by the Flv1/Flv3 heterodimer (Allahverdiyeva et al., 2013). All Flv proteins contain two redox centres, a non-heme Fe–Fe centre and a flavin mononucletide that serve as an active site and an electron accepting site, respectively. Cyanobacterial Flv contains an additional NAD(P)H: flavinoxidoreductase module at its carboxy terminus, and a recombinant protein was able to reduce O_2 to water using NAD(P)H.

Flv is wildly conserved in phototrophs from cyanobacteria to gymnosperms but not in angiosperms (Badger et al., 2003). For some unclear reasons, angiosperms have lost those proteins even if their role, apparently, could be helpful for plants. A recent work (Yamamoto et al., 2016) showed that the introduction of *Physcomytrella patens FlvA* and *FlvB* into Arabidopsis enhanced the Flv-dependent pseudoCET. In particular, the contribution of Flv as a safety valve was evident in the transgenic plants under the *pgr5* mutant background. Notably, the *pgr5* mutant was prone to photodamages under fluctuating light intensity, but the introduction of the Flv genes drastically alleviated the phenotype. Flv could form a large electron sink, when the stroma is highly reduced by electrons and protects both photosystems from photodamage in fluctuating light intensity. Although Flv may wastefully consume reducing power in the stroma under LL conditions, but the problem was not observed in the transgenic lines.

The formation of ΔpH contributes to ATP synthesis. Because proton has positive charge, Δψ also contributes to ATP synthesis. The electrochemical

gradient of proton forms pmf and consists of two components, Δψ and ΔpH. Although both components of pmf equally contribute to ATP synthesis (Soga et al., 2017), the formation of a ΔpH downregulates electron transport via acidification of the thylakoid lumen (Kanazawa and Kramer, 2002; Cruz et al., 2005). To optimize the balance of the accelerator (ATP synthesis) and brake functions, the size and component ratio of pmf should be precisely regulated.

Lumenal acidification triggers the thermal dissipation of excessively absorbed light energy from PSII antennae, a process that is monitored as an energy-dependent (qE) component of NPQ of chlorophyll fluorescence (Niyogi, 1999; Li et al., 2009; Ruban, 2016). Low lumenal pH also downregulates the rate of electron transport through the Cyt b_6f complex to slow down the electron transport toward PSI. The latter process is called photosynthetic control, and it is essential for preventing overreduction of the reaction center chlorophyll pair of PSI (P700) and, consequently, PSI photodamage.

Because the H^+/e^- (number of transferred protons per movement of an electron) is fixed in LET, CET is a main regulator of the size of pmf in angiosperms (Shikanai et al., 2014). On the other hand, ion channels and transporters localized to the thylakoid membrane modifies the ΔΨ/ΔpH ratio, by transferring H^+ or other ions across the thylakoid membrane. Recent research has focused on the identification of factors responsible for the regulation of pmf partitioning. KEA3 substitutes Δψ for ΔpH by probably coupling the efflux of H^+ with influx of K^+. KEA3 activity is especially important for optimizing the relaxation of ΔpH-dependent downregulation of photosynthetic electron transport during the induction of photosynthesis (Basso et al., 2020) and also under fluctuating light environments (Armbruster et al., 2014; Wang et al., 2017).

Although contribution of ΔpH to pmf is large especially at HL intensity in chloroplasts, mitochondrial pmf almost solely depends on Δψ. An exciting question is on the photosynthetic performance of artificial plants, which more actively use ΔΨ as a source of pmf. The systemic biological approach has been taken by Wang and Shikanai (2019), where WT and *dpgr*-type KEA3 were overexpressed in Arabidopsis to accelerate the substitution of ΔpH by Δψ. In the *dpgr* mutant, a single amino acid alteration in the 11th trans-membrane domain of KEA3 resulted in the unusually high proton leak from the thylakoid membrane (Wang et al., 2017). The overexpression of the two versions of KEA3 altered pmf. In the KEA3ox line accumulating the WT KEA3, the partitioning was leaning toward the Δψ. In contrast, in the DPGRox lines accumulating the *dpgr*-type KEA3, the size of pmf was reduced at HL intensity. The authors discussed that the high g_{H^+} (proton conductivity in the thylakoid membrane) phenotype observed in the DPGRox lines suggested the uncoupled proton leak via the mutant version of KEA3.

As reported (Armbruster et al., 2014), KEA3 is active especially after the induction of transient NPQ during the induction of photosynthesis and also

after the shift from HL to LL. This observation suggests that KEA3 is functional at moderate light intensity by balancing the partitioning of pmf components. In line with this idea, the phenotype of the KEA3ox lines was evident at moderate light intensities (101 and 331 μmol photons m^{-2} s^{-1}). The smaller contribution of ΔpH in the lines was responsible of the reduced Y(ND), allowing a higher yield of both photosystems (Wang and Shikanai 2019). However, the reduced operation of the brake at the Cyt b_6f complex made PSI more sensitive to fluctuating light intensity under the KEA3ox background. The higher contribution of Δψ to pmf might also increase the charge recombination rate in PSII, resulting in the production of singlet oxygen (Davis et al., 2016). The phenotype was even stronger in the DPGRox lines because of the reduced size of pmf (Wang and Shikanai, 2019).

In angiosperms, the regulatory system of photosynthesis has evolved in the absence of Flv (Yamamoto and Shikanai, 2017). To avoid photoinhibition of PSI, ΔpH-dependent downregulation of the Cyt b_6f complex was necessary. If angiosperms had a strong safety valve of Flv, was it possible to select the other, even better evolution? To answer this question, I combined the Flv system originated from *Physcomitrella patens* with the overexpression of WT KEA3 in Arabidopsis. In the absence of the strong ΔpH-dependent brake at the Cyt b_6f complex, PSI is hypersensitive to fluctuating light intensity (Wang and Shikanai, 2019). However, this problem could be solved by the Flv-dependent safety valve. In this chapter, I try to answer the question why angiosperms did not select this Δψ/ Flv-type photosynthesis.

2.2 MATERIALS AND METHODS

2.2.1 Plant Material and Growth Conditions

Arabidopsis thaliana WT (ecotype Columbia *gl1*), mutant plants and transgenic plants overexpressing *KEA3* and *Flv* were grown in soil in a growth chamber (50–60 µmol photons m^{-2} s^{-1}) under long-day conditions (16-h light/8-h dark cycles, 23˚C) for 3 to 4 weeks. Fully expanded leaves were used for experiments. The mutants and transgenic lines used in this study are *35Sp::KEA3* #32 (Wang et al., 2019) and Flv no. 13 (Yamamoto et al., 2016).

2.2.2 Analysis of Chlorophyll Fluorescence

Chlorophyll fluorescence parameters were measured using a MINI-PAM portable chlorophyll fluorometer (Walz) or a Dual-PAM 100 (Walz). Plants were dark adapted for 30 min before measurements. Chlorophyll fluorescence parameters were measured as described previously (Shikanai et al., 1999). The maximum quantum yield of PSII and NPQ were calculated as Fv/Fm and (Fm – Fm')/ Fm', respectively. Y(II) was calculated as (Fm – Fs)/Fm, where Fs is the steady-state fluorescence. The redox change of P700 was assessed by monitoring the absorbance changes of transmission light at 830 and 875 nm. Pm was determined by the application of an SP in the presence of far-red light (720 nm). The maximal level of P700 during AL illumination (Pm') was determined by an SP application. The steady-state P700 level, P, was recorded just before applying an SP. The quantum yield of PSI, Y(I), was calculated as (Pm'-P)/Pm. Y(NA) was calculated as (Pm-Pm')/Pm. Y(ND) was calculated as P/Pm. Three complementary quantum yields were defined: Y(I)+Y(NA)+Y(ND) = 1 (Klughammer and Schreiber, 1994). To analyze the effect of fluctuating light on photosynthetic electron transport, three repetitions of fluctuating light cycle composed of 4 min of LL (47 µmol photons m^{-2} s^{-1}) and 1 min of HL (1,529 µmol photons m^{-2} s^{-1}) were applied by changing the AL intensity, as described previously (Yamamoto et al., 2016).

2.3 RESULTS

2.3.1 The Flv-KEA3 Line Exhibits Low NPQ but high Y(ND) Phenotypes

To characterize the physiology of the double transgenic line, we analyzed a set of Arabidopsis transgenic lines. The Flvox line no. 13 (Yamamoto et al., 2016; Yamamoto et al., 2019), the KEA3ox line #32 (Wang et al., 2019) and their double transgenic line, Flv-KEA3. We analyzed the light intensity-dependence of PSI and PSII photochemistry by measuring absorption changes in P700 and chlorophyll fluorescence, respectively, using the Dual-PAM system.

Consistent with the previous report (Yamamoto et al., 2016), Y(II) was not affected in the Flv line (Fig. 2-1B). In the KEAox line, however, Y(II) was lower than in the WT. This is inconsistent with the previous observation (Wang and Shikanai, 2019), in which Y(II) was slightly higher than in the WT. The reason will be discussed below. In the Flv-KEA3 line, the Y(II) level was similar to that in the KEA3ox line, suggesting that the KEA3 level determined Y(II).

Also consistent with the previous report (Wang and Shikanai, 2019), the NPQ was mildly reduced at moderate light intensities in the KEA3ox line than in the WT (Fig. 2-1A). This phenotype was further enhanced in the Flv-KEA3 line and the maximum NPQ level at 1,200 μmol photons m^{-2} s^{-1} was also lower than that in other genotypes. The NPQ level was only slightly lower in the Flv line than in the WT.

Y(I) parameter of the P700 analysis represents the fraction of reduced P700 which can be oxidized by an SP. Y(I) is often used to estimate the quantum yield of PSI. Consistent with Y(II), the level of Y(I) was slightly reduced in the KEA3ox background (Fig. 2-2). Y(I) was also reduced to the similar level in the Flv line. Because the Y(II) level was not affected, this phenotype may reflect the competition of Flv-dependent pseudoCET with CET.

The Y(ND) parameter is calculated as the ratio of oxidized P700 ($P700^+$) per total P700 and represents the non-photochemical energy dissipation from oxidized PSI. Y(ND) is used to estimate the operation of the ΔpH-dependent downregulation of the Cyt b_6f complex (photosynthetic control), which is important to control the rate of electron transport toward PSI (Yamamoto and Shikanai, 2019). Consistent with NPQ, Y(ND) was not affected in the Flv line but was reduced in the KEA3ox line (Fig. 2-2). The results are also consistent with the previous works (Yamamoto et al., 2016; Wang and Shikanai, 2019). In the Flv-KEA3 line, however, the level of Y(ND) was higher than in that the WT. This is inconsistent with the lower NPQ phenotype observed in the Flv-KEA3 line (Fig. 2-2B). Because induction of

both NPQ and Y(ND) depends on ΔpH, we have to consider the reason other than higher contribution of Δψ to pmf to explain this discrepancy.

The acceptor side limitation of PSI, Y(NA), represents the fraction of reduced P700 that cannot be oxidized by an SP due to the lack of acceptors. The light intensity-dependence of Y(NA) showed the similar pattern in all the genotypes (Fig. 2-2C). But the Y(NA) level was slightly higher at HL intensities in the KEA3ox line than in other lines. This may be related to the lower Y(I) level observed in this line. In contrast, Y(NA) level was lower at HL intensities in the Flv-KEA3 line than in other genotypes.

Taken together these results, the Flv-KEA3 line exhibited the low NPQ but high Y(ND) phenotype. The low NPQ can be explained by the higher contribution of Δψ to pmf because of the KEA3ox but the higher Y(ND) phenotype may be explained by the strong effect of the Flv-dependent safety valve of electrons even with the lower extent of the ΔpH-dependent brake at the Cyt b_6f complex. The benefits of the single transgene didn`t affect the benefits of the other, resulting in the improvement of the phenotype in specific conditions without an additional effect of the two transgene.

2.3.2 Photosynthetic Performance of the KEA3ox-Flv line under Fluctuating Light Intensity

The Flv-KEA3 double transgenic line was subjected to the fluctuating light conditions, in which 4-min LL (45 μmol photons m^{-2} s^{-1}) period was followed by 1-min HL (996 μmol photons m^{-2} s^{-1}) period in three cycles. Because immediately after the shift from LL to HL plants cannot control the input of electrons into the intersystem, this fluctuation in light intensity is stressful for plants. Primary target of photodamage in the fluctuating light intensity is PSI rather than PSII (Yamori et al., 2016). Reaction center of PSI is transiently reduced by electrons immediately after the shift from LL to HL, resulting in the irreversible photodamage of PSI. Electrons trapped in the PSI reaction centre can be monitored as an increase in the Y(NA) parameter of the P700 analysis (Klughammer et al., 2013). To avoid the PSI photodamage, the ΔpH-dependent downregulation of the Cyt b_6f plays crucial function (Tikhonov et al., 2013). Flv forms a large electron sink from PSI and alleviates the photodamage of PSI under fluctuating light intensity (Allahverdiyeva et al., 2013). The KEA3ox lines were sensitive to fluctuating light intensity, because of the lower operation of the brake at the Cyt b_6f complex due to lower contribution of ΔpH to pmf (Wang and Shikanai, 2019).

NPQ was transiently induced in the initial LL phase but was relaxed 2 min after the induction of photosynthesis (Fig. 2-3A). The level of the transient NPQ was higher in the Flv background. After the shift from HL to LL, relaxation of NPQ was faster in the KEA3ox line (Fig. 2-3A). This is consistent with the function of KEA3 in the rapid relaxation of NPQ (Wang et al., 2017). The similar phenotype was observed also in the Flv line. This

observation is likely related to the smaller size of NPQ induced in the HL phase. Most likely, operation of Flv-dependent pseudoCET may compete with CET, resulting in the less efficient ΔpH formation in HL and more rapid relaxation of NPQ after shift to LL. This idea is consistent with the lower NPQ in the Flv-KEA3 than in the KEA3ox line under the constant light (Fig. 2-1A). In the Flv-KEA3 line, the relaxation of NPQ was more rapid than in the single transgenic lines. This phenotype may be beneficial for plants by maintaining the higher CO_2 fixation rate just after the shift from HL to LL.

Because the target of photodamage under fluctuating light intensity is PSI, Y(I) can be used to monitor the extent of PSI photodamage (Fig. 2-4A). In the LL period, Y(I) was most severely reduced in the KEA3ox line. In contrast, Y(I) was not reduced in the Flv line. In the Flv-KEA3 line, Y(I) level was restored to the WT level. Notably, Y(I) was reduced in the HL period in the Flv background, probably reflecting the competition between Flv-dependent pseudoCET and CET. Because PSII is secondarily impaired by the PSI photodamage, Y(II) was more tolerant than Y(I) to fluctuating light intensity (Figs. 2-3B and 2-4A). The decline Y(II) showed the same pattern with Y(I), suggesting that PSII was also photodamaged.

Activation of photosynthetic control is monitored as the induction of Y(ND). In the WT, induction of Y(ND) to the maximum level took 80 s in the first HL period (Fig. 2-4B). The induction of Y(ND) was complementary to that of Y(NA) reflecting the acceptor limitation from PSI (Fig. 2-4C). Even in the WT, Y(NA) was transiently induced and then relaxed within 40 s. In the KEA3ox lines, induction of Y(ND) was reduced especially in the second and third HL periods, reflecting the lower contribution of ΔpH to pmf. This was followed by a high level of transient (NA) and this should be the reason for the sensitivity of PSI to fluctuating light intensity in the KEA3ox line (Fig. 2-4C). In contrast, the maximum level of Y(ND) was induced within 20 s in the Flv line and the same pattern was observed in the Flv-KEA3 line (Fig. 2-4B). Consistently, Y(NA) level was lower in the HL period than in the LL period in the Flv background, reflecting the large size of electron sink from PSI, as reported previously (Yamamoto et al., 2016). The Y(NA) level in the LL period was higher in the Flv-KEA3 line than that in the Flv line but was similar to the WT level (Fig. 2-4C).

In the Flv-KEA3 line, relaxation of NPQ was faster after the shift from HL to LL in the order of Flv-KEA3>Flv>KEA3ox>WT (Fig. 2-1A). This phenotype may be beneficial for plants by sustaining the higher level of CO_2 fixation rate in the LL period. However, the kEA3ox line was more sensitive to fluctuating light intensity (Fig. 2-3). Introduction of Flv into the KEA3ox background restored the sensitivity of PSI to fluctuating light intensity to the WT level. The Flv-KEA3 line could took over the benefits from both single transgenic lines. This phenotype may give this line a growth benefit under the fluctuating light conditions.

2.4 DISCUSSION

In this chapter, I introduced Flv originated from *Physcomitrella patens* into the KEA3ox background to test the impact of the combination of two artificial genetic modifications on the photosynthetic performance. Wang and Shikanai (2019) reported the higher yields of both photosystems in the KEA3ox lines because of the higher contribution of $\Delta\psi$ to pmf. The problem of PSI photodamage observed in this transgenic plant may be solved by the introduction of the strong safety valve of electrons depending on Flv. However, I could not observe the expected elevated yields of both photosystems in the KEA3ox line even in the original KEA3ox line in this study (Fig. 2-1B). I am unsure the reason for this discrepancy but notably the Y(NA) level was higher in the KEA3ox line than in other genotypes, suggesting the acceptor limitation from PSI. The high Y(I) and Y(II) phenotypes of the KEA3ox line may have to be accompanied by the high CO_2 fixation activity and consequently, the phenotype may be affected by even subtle differences in the physiological conditions of plants. In this study, however, we could confirm the contribution of overaccumulating KEA3 in low NPQ and low Y(ND) (Figs. 2-1A and 2-2B). Consequently, PSI was severely photodamaged under fluctuating light intensity, as reported in Wang and Shikanai (2019).

We monitored a faster relaxation of NPQ after the shift from HL to LL in the KEA3ox line, the phenotype that was evident after the second and third HL periods. This phenotype was overlooked in the previous study (Wang and Shikanai, 2019). Because KEA3 is involved in the rapid relaxation of ΔpH-dependent downregulation of electron transport, this phenotype is simply explained by the overaccumulation of KEA3. Consistent with this idea, the knockout of *KEA3* resulted in the delay in the relaxation of NPQ after the shift from HL to LL (Wang and Shikanai, 2019). Unexpectedly, relaxation of NPQ after the shift from HL to LL was accelerated also in the Flv line (Fig. 2-3A). This phenotype was further enhanced in the Flv-KEA3 line, in which NPQ was relaxed to the LL level within 20 s after the shift to LL. How does Flv contribute to the rapid relaxation of NPQ? The Flv-dependent pseudoCET may compete with CET in the HL period. Because CET is more efficient for ΔpH formation than pseudoCET, lower activity of CET may have contributed to the rapid relaxation of NPQ in the Flv background. This idea is supported by the low Y(I) in the LL phase observed in the Flv background (Fig. 2-4A). To maintain the high rate of CO_2 fixation under fluctuating light intensity, a successful strategy of the artificial gene modification is the overaccumulation of zeaxanthin epoxidase to rapidly relax zeaxanthin-dependent NPQ after the shift from HL to LL (Kromdijk et al., 2016). We may be able to expect the similar impact in the combination of KEA3ox and Flv.

Even though the KEA3ox provides the positive trait of utilizing light energy more efficiently, a serious problem is excessive electron flow toward

PSI after the shift from LL to HL. This causes a serious photodamage of PSI (Wang and Shikanai, 2019) Our strategy was the rebalancing of this trade-off by the introduction of Flv. Flv may be able to efficiently work as an electron sink from PSI, as its introduction restored the sensitivity of PSI to fluctuating light intensity in the *pgr5* mutant background (Yamamoto et al., 2016). In the Flv-KEA3 line, almost all the parameters were recovered to the WT levels under the fluctuating light conditions (Figs. 2-3 and 2-4). However, PSI was more resistant to fluctuating light intensity in the Flv line than in Flv-KEA3 line, as evident in the Y(I) levels (Fig. 2-4). Even with the strong safety valve of Flv, the KEA3ox led to the photodamage to PSI under fluctuating light intensity to some extents. A question is whether the Flv-KEA3 line is superior to the Flv line or the WT? This question is related to how the rapid relaxation of NPQ contribute to keep the CO_2 fixation level higher under fluctuating light intensity in the Flv-KEA3 line. Although we could not reproduce the high Y(I) and Y(II) phenotypes in the KEA3ox background, recovery of Y(II) was faster in the FLV-KEA3 line than in the WT (Fig. 2-3B). LET may be accelerated in the KEA3ox background. How does this positive utilization of light energy contribute to the net fixation of CO_2 in the KEA3ox background? We are planning to evaluate the rate of CO_2 fixation under the fluctuating light conditions. It may be also important to compare the growth phenotype among the genotypes under the fluctuating light conditions. In the analysis of photosynthesis under constant light (Figs. 2-1 and 2-2), the impact of the two transgenes explain the phenotypes observed under the fluctuating light intensity. The NPQ level was lower in the Flv-KEA3 line under HL (>100 μmol photons m^{-2} s^{-1}) and was even lower than in the KEA3ox (Fig. 2-3A). On the other hand, Y(ND) was higher in the Flv-KEA3 line than in the WT (Fig. 2-4B). Because both NPQ and Y(ND) depend on ΔpH for the induction, this observation was somewhat unexpected. We consider that contribution of Δψ to pmf is enhanced under the KEA3ox background but the larger electron sink depending on Flv functions to keep P700 oxidized even with lower activity of the brake at the Cyt b_6f complex. The impact of one transgene does not exclude the function of the other transgene mutually. More research is needed to conclude whether the Flv-KEA3 line is superior to the WT.

INTEGRATED DISCUSSION AND OUTLOOK

Chemical gradients are a seminal component for the synthesis of energy in many organisms. In the chloroplast, the combination of ΔpH and Δψ contributes to ATP synthesis as pmf. In contrast, Δψ predominately contributes to pmf in mitochondria. This character of pmf components in chloroplasts plays a regulatory role in the balancing of an accelerator (ATP synthesis) and a brake downregulating the electron transport. The regulatory network may be even more complicated, because Δψ also seems to be involved in the regulatory processes, such as the gating of some channels or the uptake of some metabolites (Szabo, 2017). In the last decade, our knowledge on the molecular mechanism for regulating the size of pmf has been progressed depending on the discovery of two CET pathways (Yamori and Shikanai, 2016). However, the information of the regulatory machinery for the pmf components, channels and transporters, has been still limited (Spetea et al., 2017). We still cannot imagine the entire model of regulatory network for the pmf regulation.

Recent physiology on the protection mechanism against excessive light has focused on the fluctuation in light intensity rather than the response to constant HL. In my study, clear phenotypes of the mutants and the transgenic lines were also observed under fluctuating light intensity. This is because the regulation of pmf is closely related to the optimization of the trade-off between the accelerator (more positive utilization of light energy) and the brake (photoprotection).

I have started my Ph.D. study taking a genetic approach to understand the crosstalk between the regulatory machinery (Chapter 1). The NDH complex seemed to be able to shift between its canonical proton pumping activity (CET) and the proposed reverse activity to alleviate the pressure from the overreduction of the PQ pool and too large ΔpH. This discovery depended on the analysis of plants under the *kea3-1* mutant background. The regulatory sytem of pmf is likely complementary each other and the analysis of double mutants may be effective to reveal the molecular basis of the network. Subsequently, I extended my approach to systemic biology (Chapter 2), because some recent works have drastically and successfully modified the fundamental regulatory systems (Yamamoto et al., 2016; Wang and Shikanai, 2019). We may be able to understand why angiosperms have selected this evolution rather than the other, maybe even better one. The phenotypes of the Flv-KEA3 double transgenic line were somewhat different from our original estimation from those in each original transgenic line but was more insightful for the reason why angiosperms selected CET instead of Flv-dependent peudoCET. The genetic engineering potentially improves the performance of photosynthesis (Kromdijk et al., 2016) but the simple enhancement of photosynthetic activity has not been successful so far. However, the phenotype of the Flv-KEA3 line suggests that it may be possible

to replace the fundamental regulatory machinery drastically and this approach may lead to the creation of “new photosynthesis”.

Through two chapters, I showed how the regulation of pmf is optimized in response to the fluctuating light environments and how the different regulatory systems collaborate each other for fine-tuning the regulation. I realized that we are still in the stage of understanding the molecular basis of the regulatory network. But it may not be very difficult to artificially modify the regulatory network. Overall, the trade-off between the accelerator and the brake function is delicate and has been already optimized to some extents at least. However, Flv and the NDH complex contribute to the flexibility of the regulation, permitting the rather drastic alteration of the regulatory network.

ACKNOWLEDGEMENT

This work would have not been possible without many people that supported me, both professionally and personally, during the last three years.

I cannot begin to express my appreciation to Shikanai Sensei who accepted me in his lab and invested his energy on the guiding me through the Ph.D., shaping me as the scientist I am now. I am also grateful to Tsugeki sensei that encouraged me throughout the duration of this project, particularly, during the second year: I made treasure of the words you told me.

The completion of my Ph.D. would have not been possible without the financial support of the "Human Life Advancement Foundation". Thank you for having invested in me during the last years.

Thanks, should also go to Kato san for all the valuable advices when I first arrived in this laboratory: I learned so many techniques under your guidance.

I would like to recognize the assistance that I received from Sachi san, Yamamoto san and all the other lab members: all the good and bad moments we had together shaped my experience in this lab. I cannot leave this laboratory without mentioning Brody, the best lab buddy I could ask, that supported me during all the mood swing that a science sometimes gives.

This work was also supported by many people outside of the lab, among them, I wish to acknowledge Linda, Davide, Michele, Dafne and Nicolò for bearing me when I was grumpier than usually and for all the memories we could create since this adventure began.

To conclude, my deepest appreciation goes to my family: Samuela, Eddy, Stefania, Gregorio, Giorgia and Nicola for all the unconditional support despite the distance.

BIBLIOGRAPHY

Allahverdiyeva Y, Mustila H, Ermakova M, Bersanini L, Richaud P, Ajlani G, Battchikova N, Cournac L, Aro E-M (2013) Flavodiiron proteins Flv1 and Flv3 enable cyanobacterial growth and photosynthesis under fluctuating light. Proc. Natl. Acad. Sci. USA **110:** 4111–4116.

Allahverdiyeva Y, Isojärvi J, Zhang P, Aro E-M (2015) Cyanobacterial oxygenic photosynthesis is protected by flavodiiron proteins. Life (Basel) **5:** 716–743.

Armbruster U, Carrillo LR, Venema K, Pavlovic L, Schmidtmann E, Kornfeld A, Jahns P, Berry JA, Kramer DM, Jonikas MC (2014) Ion antiport accelerates photosynthetic acclimation in fluctuating light environments. Nat. Commun. **5:** 5439.

Asada K (1999) The water-water cycle in chloroplasts: scavenging of active oxygens and dissipation of excess photons. Annu. Rev. Plant Physiol. Plant Mol. Biol. **50:** 601–639.

Asada K (2000) The water-water cycle as alternative photon and electron sinks. Philo. Trans. R. Soc. Lond. B. Biol Sci. **355:** 1419–1431.

Badger MR, von Caemmerer S, Ruuska S, Nakano H (2000) Electron flow to oxygen in higher plants and algae: rates and control of direct photoreduction (Mehler reaction) and rubisco oxygenase. Philos. Trans. R. Soc. Lond. B **355:** 1433–1446.

Bailleul B, Cardol P, Breyton C, Finazzi G (2010) Electrochromism: a useful probe to study algal photosynthesis. Photosynth. Res. **106:** 179–189.

Basso L, Yamori W, Szabo I, Shikanai T (2020) Collaboration between NDH and KEA3 allows maximally efficient photosynthesis after a long dark adaptation. Plant Physiol. **184:** 2078–2090.

Bednarczyk P, Wieckowski MR, Broszkiewicz M, Skowronek K, Siemen D, Szewczyk A. (2013) Putative structural and functional coupling of the mitochondrial BK channel to the respiratory chain. PloS one **8:** e68125.

Bloom AJ, Lancaster KM (2018) Manganese binding to Rubisco could drive a photorespiratory pathway that increases the energy efficiency of photosynthesis. Nat. Plants **4:** 414–422.

Buchanan BB (2016) The path to thioredoxin and redox regulation in chloroplasts. Annu. Rev. Plant Biol. **67:** 1–24.

Cruz JA, Sacksteder CA, Kanazawa A, Kramer DM (2001) Contribution of electric field (Δψ) to steady-state trans thylakoid proton motive force (pmf) in vitro and in vivo. Control of pmf parsing into Δψ and ΔpH by ionic strength. Biochemistry **40:** 1226–1237.

DalCorso G, Pesaresi P, Masiero S, Aseeva E, Schünemann D, Finazzi G, Joliot P, Barbato R, Leister D (2008) A complex containing PGRL1 and PGR5 is involved in the switch between linear and cyclic electron flow in Arabidopsis. Cell **132:** 273–285.

Elbehti A, Brasseur G, Lemesle-Meunier D (2000) First evidence for existence of an uphill electron transfer through the bc_1 and NADH-Q oxidoreductase complexes of the acidophilic obligate chemolithotrophic ferrous ion-oxidizing bacterium *Thiobacillus ferrooxidans*. J. Bacteriol. **182:** 3602–3606.

Ferro M, Brugiere S, Salvi D, Seigneurin D, Magali B Court, Moyet L, Ramus C Miras S Mellal M, Le Gall S, Kieffer-Jaquinod S, Bruley C, Garin J, Joyard J, Masselon C, and Rolland N (2010) AT_CHLORO, a comprehensive chloroplast proteome database with subplastidial localization and curated information on envelope proteins. Mol. Cell Proteomics **9:** 1063–1084.

Hashimoto M, Endo T, Peltier G, Tasaka M, Shikanai T (2003) A nucleus-encoded factor, CRR2, is essential for the expression of chloroplast *ndhB* in Arabidopsis. Plant J. **36:** 541–549.

Havaux M, Niyogi KK (1999) The violaxanthin cycle protects plants from photooxidative damage by more than one mechanism. Proc. Natl. Acad. Sci. USA. **96:** 8762–8767.

Helman Y. Tchernov D, Reinhold L, Shibata M, Ogawa T, Schwarz R, Ohad I and Kaplan A (2003) Genes encoding A-type flavoproteins are essential for photoreduction of O2 in cyanobacteria. Curr. Biol. 13: 230–235.

Herter SM, Kortlüke CM, Drews G (1998) Complex I of *Rhodobacter capsulatus* and its role in reverted electron transport. Arch. Microbiol. **169:** 98–105.

Ifuku K, Endo T, Shikanai T, Aro E-M (2011) Structure of the chloroplast NADH dehydrogenase-like complex: nomenclature for nuclear-encoded subunits. Plant Cell Physiol. **52:** 1560–1568.

Kramer DM, Cruz JA, Kanazawa A (2003) Balancing the central roles of the thylakoid proton gradient. Trends Plant Sci. **8:** 27–32.

Kramer DM, Johnson G, Kiirats O, Edwards GE (2004) New fluorescence parameters for the determination of Q_A redox state and excitation energy fluxes. Photosynth. Res. **79:** 209–218.

Kromdijk J, Głowacka K, Leonelli L, Gabilly ST, Iwai M, Krishna K. Niyogi, Long S (2016) Improving photosynthesis and crop productivity by accelerating recovery from photoprotection. Science **354:** 857-861.

Klughammer C, Schreiber U (1994) An improved method, using saturating light pulses, for the determination of photosystem I quantum yield via $P700^+$-absorbance changes at 830 nm. Planta **192:** 261–268.

Klughammer C, Siebke K, Schreiber U (2013) Continuous ECS-indicated recording of the proton-motive charge flux in leaves. Photosynth. Res. **117:** 471–487.

Kohzuma K, Dal Bosco C, Meurer J, Kramer DM (2013) Light- and metabolism-related regulation of the chloroplast ATP synthase has distinct mechanisms and functions. J. Biol. Chem. **288:** 13156–13163.

Kunz H-H, Gierth M, Herdean A, Satoh-Cruz M, Kramer DM, Spetea C, Schroeder JI (2014) Plastidial transporters KEA1, -2, and -3 are essential for chloroplast osmoregulation, integrity, and pH regulation in Arabidopsis. Proc. Natl. Acad. Sci. USA **111:** 7480–7485.

Li Z, Wakao S, Fischer BB, Niyogi KK (2009) Sensing and responding to excess light. Annu. Rev. Plant Biol. **60:** 239–260.

Motohashi K, Kondoh A, Stumpp MT, Hisabori T (2001) Comprehensive survey of proteins targeted by chloroplast thioredoxin. Proc. Natl. Acad. Sci. USA **98:** 11224–11229.

Müller P, Li XP, Niyogi KK (2001) Non-photochemical quenching. A response to excess light energy. Plant Physiol. **125:** 1558–1566.

Munekage Y, Hojo M, Meurer J, Endo T, Tasaka M, Shikanai T (2002) PGR5 is involved in cyclic electron flow around photosystem I and is essential for photoprotection in Arabidopsis. Cell **110:** 361–371.

Munekage Y, Hashimoto M, Miyake C, Tomizawa K, Endo T, Tasaka M, Shikanai T (2004) Cyclic electron flow around photosystem I is essential for photosynthesis. Nature **429:** 579–582.

Nakano H, Yamamoto H, Shikanai T (2019) Contribution of NDH-dependent cyclic electron transport around photosystem I to the generation of proton motive force in the weak mutant allele of *pgr5*. Biochim. Biophys. Acta Bioenergetics **1860:** 369–374.

Nikkanen L, Toivola J, Trotta A, Diaz MG, Tikkanen M, Aro E-M, Rintamäki E (2018) Regulation of cyclic electron flow by chloroplast NADPH-dependent thioredoxin system. Plant Direct **2:** e00093.

Nikkanen L, Sanchez AS, Ermakova M, Rögner M, Cournac L, Allahverdiyeva Y (2020) Functional redundancy between flavodiiron proteins and NDH-1 in *Synechocystis* sp. PCC 6803. Plant J. doi: 10.1111/tpj.14812.

Okegawa Y, Long TA, Iwano M, Takayama S, Kobayashi Y, Covert SF, Shikanai T (2007) A balanced PGR5 level is required for chloroplast

development and optimum operation of cyclic electron transport around photosystem I Plant Cell Physiol. **48:** 1462–1471.

Peltier G, Aro E-M, Shikanai T (2016) NDH-1 and NDH-2 plastoquinone reductases in oxygenic photosynthesis. Annu. Rev. Plant Biol. **67:** 55–80.

Roosild TP, Miller S, Booth IR, Choe S (2002) A mechanism of regulating transmembrane potassium flux through a ligand-mediated conformational switch. Cell **109:** 781–791.

Ruban AV (2016) Nonphotochemical chlorophyll fluorescence quenching: Mechanism and effectiveness in protecting plants from photodamage. Plant Physiol. **170:** 1903–1916.

Schlosser A, Hamann A, Bossemeyer D, Schneider E, Bakker EP (1993) NAD^+ binding to the *Escherichia coli* K^+-uptake protein TrkA and sequence similarity between TrkA and domains of a family of dehydrogenases suggest a role for NAD^+ in bacterial transport. Mol. Microbiol. **9:** 533–543.

Shikanai T (2007) Cyclic electron transport around photosystem I: genetic approaches. Annu. Rev. Plant Biol. **58:** 199–217.

Shikanai T (2014) Central role of cyclic electron transport around photosystem I in the regulation of photosynthesis. Curr. Opin. Biotech. **26:** 25–30.

Shirao M, Kuroki S, Kaneko K, Kinjo Y, Tsuyama M, Förster B, Takahashi S, Badger M (2013) Gymnosperms have increased capacity for electron leakage to oxygen (Mehler and PTOX reactions) in photosynthesis compared with angiosperms. Plant Cell Physiol. **54:** 1152–1163.

Soga N, Kimura K, Kinosita K Jr, Yoshida M, Suzuki T (2017) Perfect chemomechanical coupling of FoF1-ATP synthase. Proc. Natl. Acad. Sci. USA **114:** 4960–4965.

Spetea C, Herdean A, Allorent G, Carraretto L, Finazzi, Szabo I (2017) An update on the regulation of photosynthesis by thylakoid ion channels and transporters in Arabidopsis. Physiol. Plant **161:** 16–27.

Stiehl HH, Witt HT (1969) Quantitative treatment of the function of plastoquinone in photosynthesis. Z. Naturforsch B **24:** 1588–1598.

Strand DD, Fisher N, Kramer DM (2017) The higher plant plastid NAD(P)H dehydrogenase-like complex (NDH) is a high efficiency proton pump that increases ATP production by cyclic electron flow. J. Biol. Chem. **292:** 11850–11860.

Suorsa M, Järvi S, Grieco M, Nurmi M, Pietrzykowska M, Rantala M, Kangasjärvi S, Paakkarinen V, Tikkanen M, Jansson S, Aro E-M (2012) PROTON GRADIENT REGULATION5 is essential for proper acclimation of Arabidopsis photosystem I to naturally and artificially fluctuating light conditions. Plant Cell **24:** 2934–2948.

Szabò I, Spetea C. (2017) Impact of the ion transportome of chloroplasts on the optimization of photosynthesis. J. Exp. Bot. **68:** 3115–3128.

Takabayashi A, Ishikawa N, Obayashi T, Ishida S, Obokata J, Endo T, Sato F (2009) Three novel subunits of Arabidopsis chloroplastic NAD(P)H dehydrogenase identified by bioinformatic and reverse genetic approaches. Plant J. **57:** 207–219.

Takizawa K, Kanazawa A, Kramer DM (2008) Depletion of stromal P_i induces high "energy-dependent" antenna exciton quenching (q_E) by decreasing proton conductivity at CF_O-CF_1 ATP synthase. Plant Cell Environ. **31:** 235–243.

Tikkanen M, Grieco M, Kangasjärvi S, Aro E-M (2010) Thylakoid protein phosphorylation in higher plant chloroplasts optimizes electron transfer under fluctuating light. Plant Physiol. **152:** 723–735.

Tsujii M, Kera K, Hamamoto S, Kuromori T, Shikanai T, Uozumi N (2019) Evidence for potassium transport activity of Arabidopsis KEA1-KEA6. Sci. Rep. **11:** 10040.

Ueda M, Kuniyoshi T, Yamamoto H, Sugimoto K, Ishizaki K, Kohchi T, Nishimura Y, Shikanai T (2012) Composition and physiological function of the chloroplast NADH dehydrogenaselike complex in Marchantia polymorpha. Plant J. **72:** 683–693.

Wang C, Shikanai T (2019) Modification of activity of the thylakoid H^+/K^+ antiporter KEA3 disturbs ΔpH-dependent regulation of photosynthesis. Plant Physiol. **181:** 762–773.

Wang C, Yamamoto H, Shikanai T (2015) Role of cyclic electron transport around photosystem I in regulating proton motive force. Biochim. Biophys. Acta **1847:** 931–938.

Wang C, Yamamoto H, Narumiya F, Munekage YN, Finazzi G, Szabo I, Shikanai T (2017) Fine-tuned regulation of the K^+/H^+ antiporter KEA3 is required to optimize photosynthesis during induction. Plant J. **89:** 540–553.

Wojtovich AP, Smith CO, Haynes CM, Nehrke KW, Brookes PS (2013) Physiological consequences of complex II inhibition for aging, disease, and the mKATP channel. Biochim. Biophys. Acta **1827:** 598–611.

Yamamoto H, Shikanai T (2019) PGR5-dependent cyclic electron flow protects photosystem I under fluctuating light at donor and acceptor sides. Plant Physiol. **179:** 588–600.

Yamamoto H, Takahashi S, Badger MR, Shikanai T (2016) Artificial remodeling of alternative electron flow by flavodiiron proteins in Arabidopsis. Nat. Plants **2:** 16012.

Yamori W, Shikanai T (2016) Physiological functions of cyclic electron transport around photosystem I in sustaining photosynthesis and plant growth. Annu. Rev. Plant Biol. **67:** 81–106.

Yamori W, Shikanai T, Makino A (2015) Photosystem I cyclic electron flow via chloroplast NADH dehydrogenase-like complex performs a physiological role for photosynthesis at low light. Sci. Rep. **5:** 13908.

Yamori W, Makino A, Shikanai T (2016) A physiological role of cyclic electron transport around photosystem I in sustaining photosynthesis under fluctuating light in rice. Sci. Rep. **6:** 20147.

TABLES

Table 1A

Figures	parameter	Time point	WT	*pgr5-1*	*kea3-1*	*kea3-1 pgr5-1*
Fig. 1-1A	NPQ	1 min	a	b **	a	b **
Fig. 1-1B	Y(II)	1 min	a	b **	a	b**

Different letters indicate the statistical differences confirmed by the Tukey-Kramer test (P < 0.05). Asterisks indicate a statistically significant difference from WT (*P < 0.05, **P < 0.01), confirmed by the Dunnett test.

Table 1B

Figures	parameter	Time point	WT	*crr2-1*	*kea3-1*	*crr2-1 kea3-1*
Fig. 1-1C	NPQ	2 min	a	a	a*	b **
Fig. 1-1D	Y(II)	2 min	a	a	a	b **

Different letters indicate the statistical differences confirmed by the Tukey-Kramer test (P < 0.05). Asterisks indicate a statistically significant difference from WT (*P < 0.05, **P < 0.01), confirmed by the Dunnett test.

Table 2

Figures	parameter	Time point	WT	*crr2-1*	*kea3-1*	*crr2-1 kea3-1*
Fig. 1-2A	NPQ	2 min	a	a	b*	b **
Fig. 1-2B	Y(II)	2 min	a	ab*	b**	c **

Different letters indicate the statistical differences confirmed by the Tukey-Kramer test (P < 0.05). Asterisks indicate a statistically significant difference from WT (*P < 0.05, **P < 0.01), confirmed by the Dunnett test.

Table 3

Figures	parameter	Time point	WT	*pnsb2*	*kea3-1*	*kea3-1pnsb2*
Fig. 1-3A	NPQ	2 min	a	a	ab	b **
Fig. 1-3B	Y(II)	2 min	a	ab	ab	b**
Fig. 1-3C	Y(I)	2 min	a	a	a	a
Fig. 1-3D	Y(ND)	2 min	a	ab	ab	b**
Fig. 1-3E	Y(NA)	2 min	a	a	a	a*

Different letters indicate the statistical differences confirmed by the Tukey-Kramer test (P < 0.05). Asterisks indicate a statistically significant difference from WT (*P < 0.05, **P < 0.01), confirmed by the Dunnett test.

Table 4

Figures	parameter	Time point	WT	*crr2-1*	*kea3-1*	*crr2-1 kea3-1*
Fig. 1-5A	Y(I)	1 min	a	b**	ab	c **
Fig. 1-5B	Y(ND)	1 min	a	ab	a	b **
Fig. 1-5C	Y(NA)	1 min	a	ab*	a	b **

Different letters indicate the statistical differences confirmed by the Tukey-Kramer test (P < 0.05). Asterisks indicate a statistically significant difference from WT (*P < 0.05, **P < 0.01), confirmed by the Dunnett test.

Table 5

Figures	parameter	Time point	WT	*crr2-1*	*kea3-1*	*crr2-1 kea3-1*
Fig. 1-6A	pmf	20 s	a	b**	b**	c**
Fig. 1-6A	pmf	180 s	a	ab*	b**	ab*
Fig. 1-6B	g_{H^+}	20 s	a	a	a	a*
Fig. 1-6B	g_{H^+}	180 s	a	a	a	b**
Fig. 1-6C	pmf	20 s	a	a	a	a
Fig. 1-6C	pmf	180 s	a	a	a	a
Fig. 1-6D	g_{H^+}	20 s	a	a	a	a
Fig. 1-6D	g_{H^+}	180 s	a	a*	b	c**

Different letters indicate the statistical differences confirmed by the Tukey-Kramer test (P < 0.05). Asterisks indicate a statistically significant difference from WT (*P < 0.05, **P < 0.01), confirmed by the Dunnett test.

Table 6

Figures	parameter	Time point	WT	*crr2-1*	*kea3-1*	*crr2-1kea3-1*
Fig. 1-8A	NPQ	80 s	a	b**	a	b**
Fig. 1-8B	Y(II)	80 s	a	b**	a*	b**
Fig. 1-8C	Y(I)	80 s	a	b**	a	b**
Fig. 1-8D	Y(ND)	80 s	a	b**	a	b**

Fig. 1-8E	Y(NA)	80 s	a	b**	a	b**

Different letters indicate the statistical differences confirmed by the Tukey-Kramer test (P < 0.05). Asterisks indicate a statistically significant difference from WT (*P < 0.05, **P < 0.01), confirmed by the Dunnett test.

Table 7

Figures	parameter	Time point	WT	*crr2-1*	*35s::pgr5*	*35s::pgr5 crr2-1*
Fig. 1-10A	NPQ	3 min	a	a	a*	b **
Fig. 1-10B	Y(II)	3 min	a	ab	b**	c**
Fig. 1-10C	Y(I)	3 min	ab	ab	a	b
Fig. 1-10A	Y(ND)	3 min	a	a	b**	c **
Fig. 1-10B	Y(NA)	3 min	a	a	b**	b**

Different letters indicate the statistical differences confirmed by the Tukey-Kramer test (P < 0.05). Asterisks indicate a statistically significant difference from WT (*P < 0.05, **P < 0.01), confirmed by the Dunnett test.

Table 8

Figure	t50 (s)	WT	*crr2-1*	*kea3-1*	*crr2-1 kea3-1*
Fig. 1-12A	CO_2	113.38 ± 4.8	109.8 ± 15.9	117.1 ± 12.4	161.6 ± 9.1*
Fig. 1-13A	Y(II)	30.2 ± 3.2	36.3 ± 3.4*	30.6 ± 1.0	95.3 ± 18.2*
Fig. 1-13C	Y(I)	20.0 ± 1.7	30.0 ± 3.4	22.0 ± 1.5	55.0 ± 8.5*
Fig. 1-12B	CO_2	107.3 ± 0.7	111.1 ± 15.3	102.1 ± 4.5	119.9 ± 17.2
Fig. 1-13B	Y(II)	24.4 ± 0.8	24.7 ± 1.1	25.2 ± 1.4	29.0 ± 1.6
Fig. 1-13D	Y(I)	16.2 ± 1.1	15.9 ± 1.3	16.6 ± 0.9	18.5 ± 2.0

t50 represents time (s) needed to reach the 50% of the maximum level. Values are means ± standard errors (n=5). Asterisks indicate the statistical difference from WT (P<0.05).

FIGURES

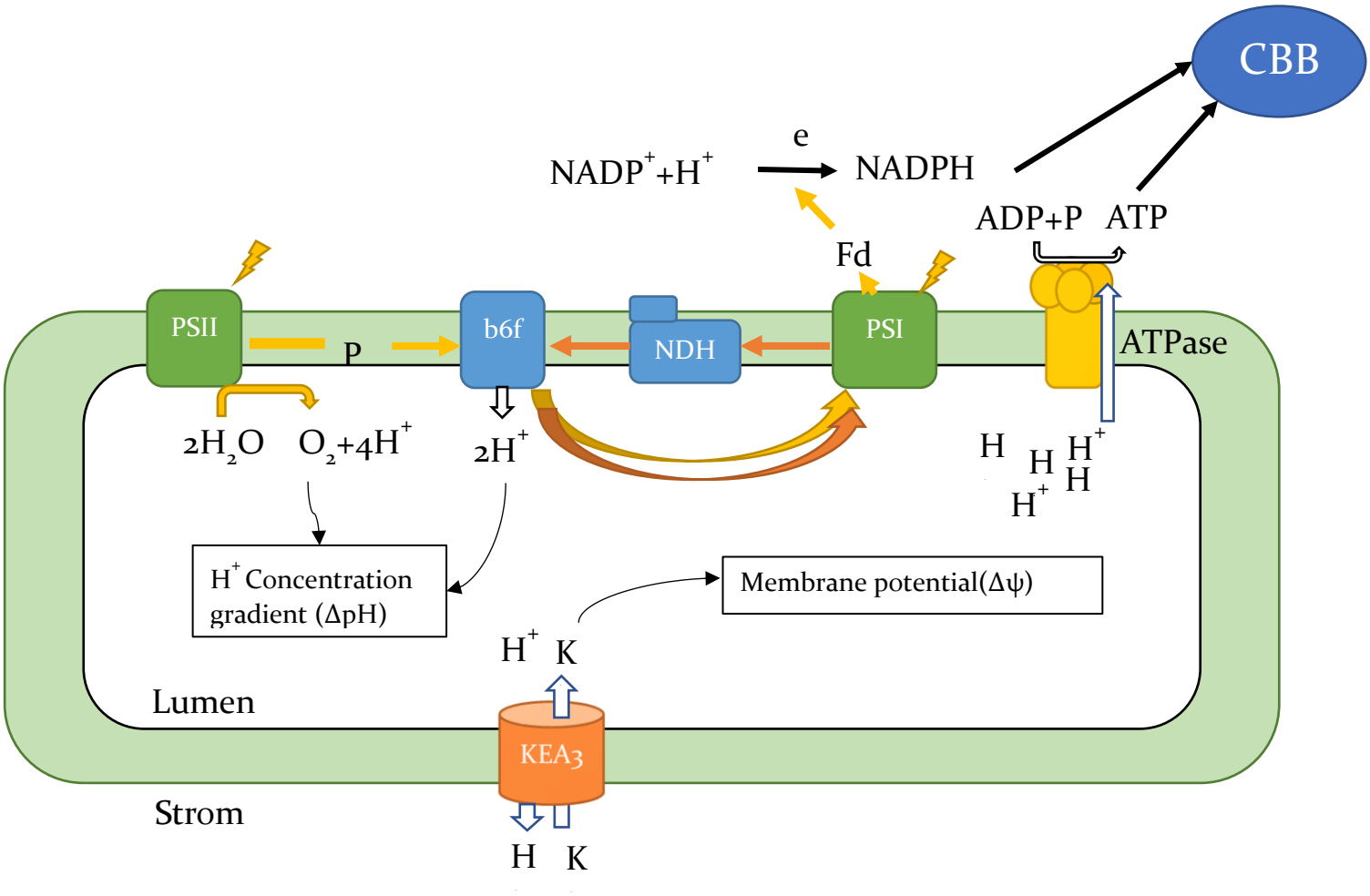

Figure 1. A schematic model of photosynthetic electron transport. LET from water to $NADP^+$ is indicated by yellow arrows. Orange arrows indicate the two CET pathways, involving PGR5/PGRL1 and the NDH complex. Flv-dependent pseudoCET is indicated by blue lines. CET and KEA3 modulate the size and component partitioning of the pmf, respectively. The pmf consists of two components of Δψ and ΔpH, which are ultimately used to drive ATP synthase activity. The pmf contribute to not only to the ATP synthesis but also to the regulation of the photosynthetic electron transport by inducing thermal dissipation from PSII, monitored as NPQ of chlorophyll fluorescence, and by downregulating the activity of the Cyt b_6f complex.

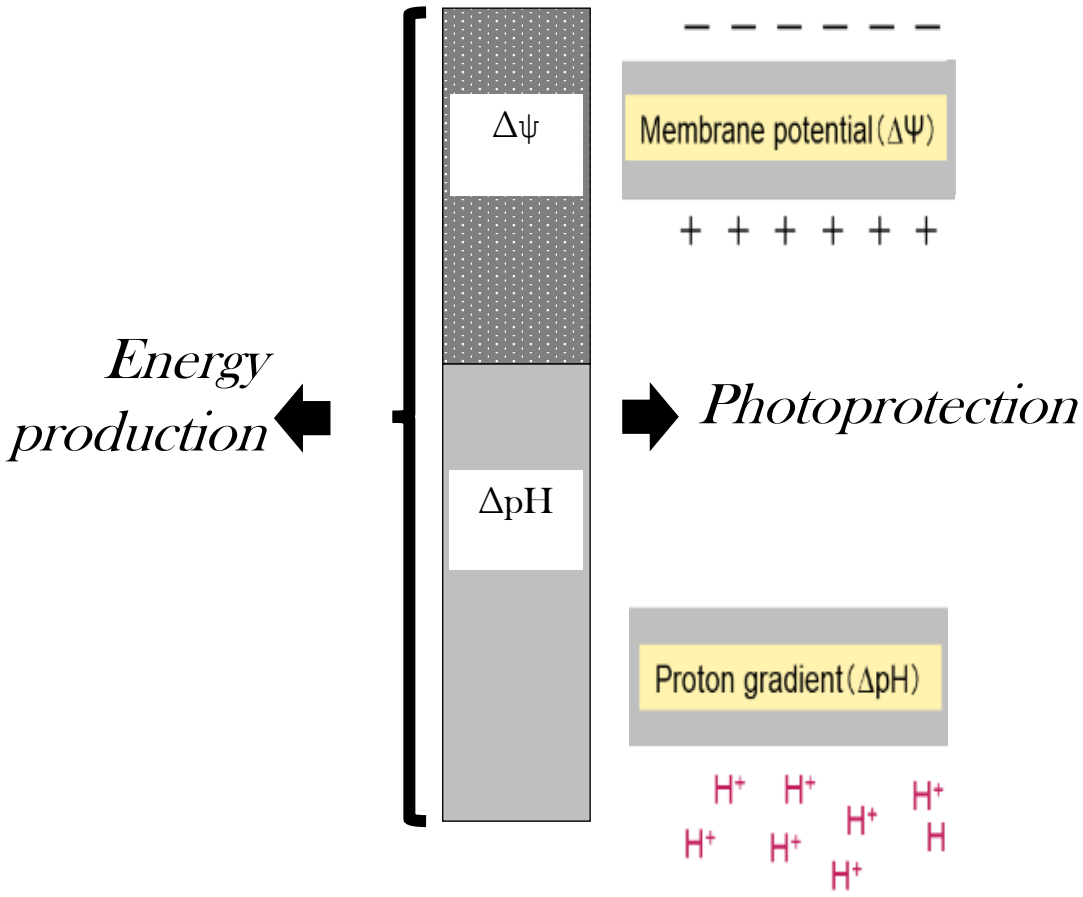

Figure 2: Component partitioning of pmf. Pmf consists of two components the proton concentration gradient (ΔpH) and the membrane potential (Δψ) represented by the uneven distribution of other ions. Both the components drive the synthesis of energy through Co-CF1-ATP synthase, but only ΔpH contributes to the photoprotection by the downregulation of the Cytb6f and the dissipation of the excessively harvested light energy from PSII antennae (NPQ).

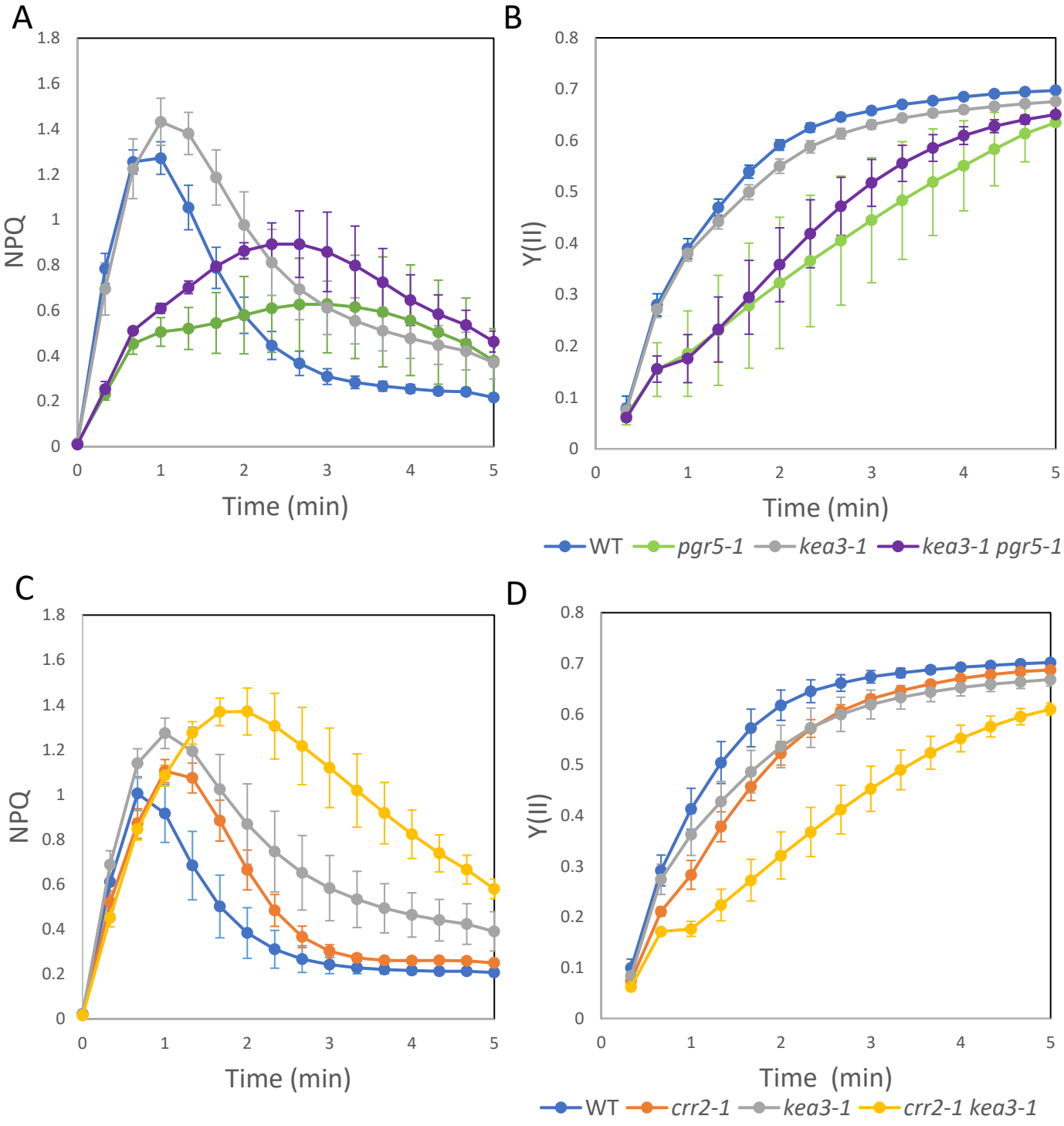

Figure 1-1. Induction of photosynthesis by non-saturating light (110 µmol photons m^{-2} s^{-1}). Induction and relaxation of NPQ (A and C) and induction of Y(II) (B and D) were measured by chlorophyll fluorescence. A set of genotypes including *kea3-1* and *pgr5-1* (A and B), and *crr2-1* and *kea3-1* (C and D) were analyzed. Data are shown as means ± standard errors (SE) (n = 4–5). Detached leaves from dark-adapted plants were exposed to AL. Triangles indicate the time points for statistical analyses summarized in Table 1.

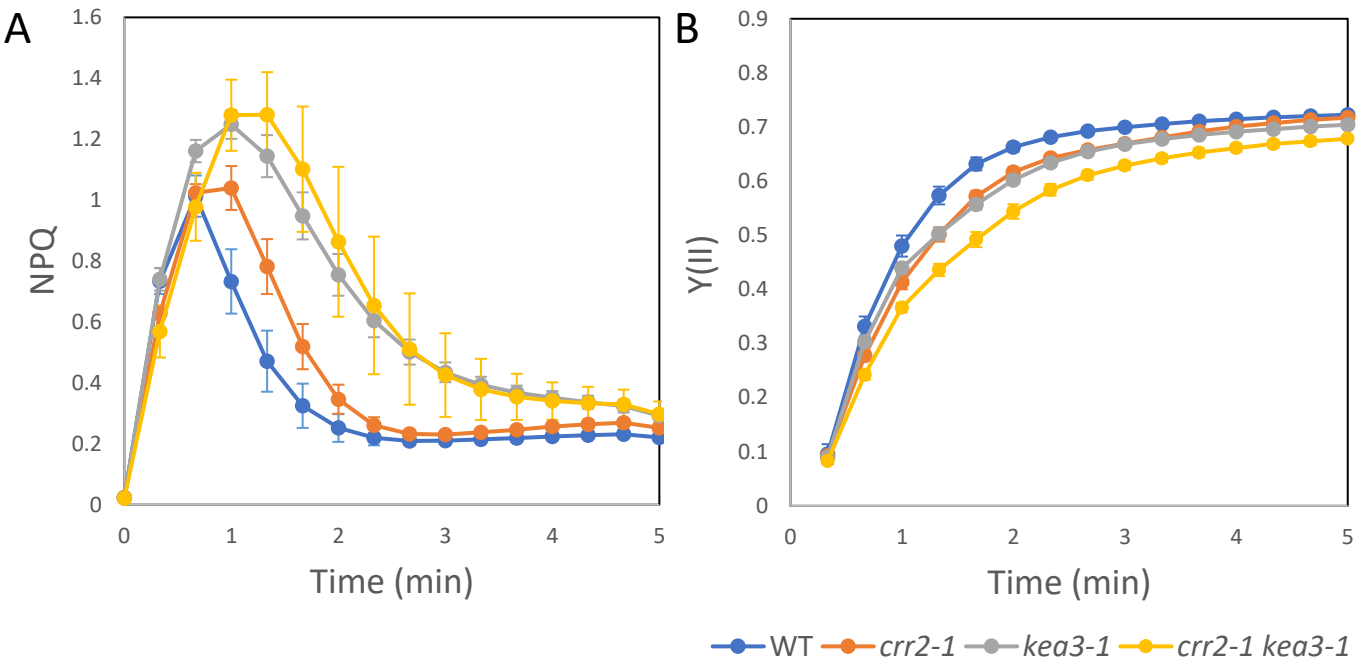

Figure 1-2. Induction of photosynthesis by non-saturating light (110 µmol photons m^{-2} s^{-1}) after 30-min dark adaptation. Induction and relaxation of NPQ (A) and induction of Y(II) (B) were measured by chlorophyll fluorescence in a set of genotypes including *crr2-1* and *kea3-1*. Data are shown as mean ± SE (n = 4–5). Detached leaves from dark-adapted plants were exposed to AL. Triangles indicate the time point (2 min) for statistical analyses summarized in Table 2.

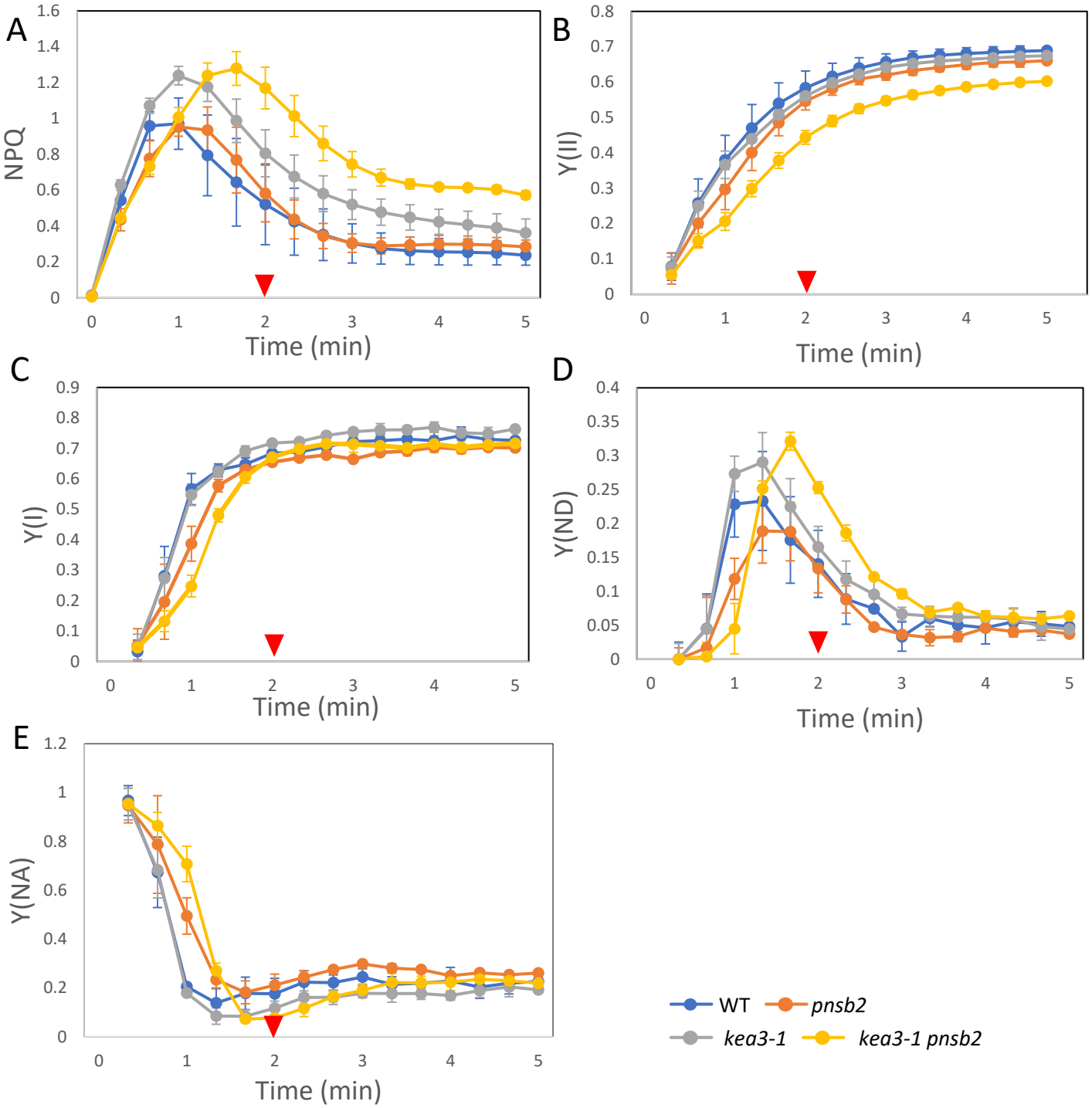

Figure 1-3. Induction of photosynthesis under non-saturating light (110 µmol photons m^{-2} s^{-1}) after overnight dark adaptation. Induction and relaxation of NPQ (A) and induction of Y(II) (B) were measured by chlorophyll fluorescence in a set of genotypes including *pbsb2* and *kea3-1*. Yields of PSI, Y(I) (C), donor-side regulation of PSI, Y(ND) (D) and acceptor-side limitation of PSI, Y(NA) (E) were also analyzed by monitoring the P700 absorbance changes. Data are shown as mean ± SE (n = 3). Detached leaves from dark-adapted plants were exposed to AL. Triangles indicate the time point (2 min) for statistical analyses summarized in Table 4.

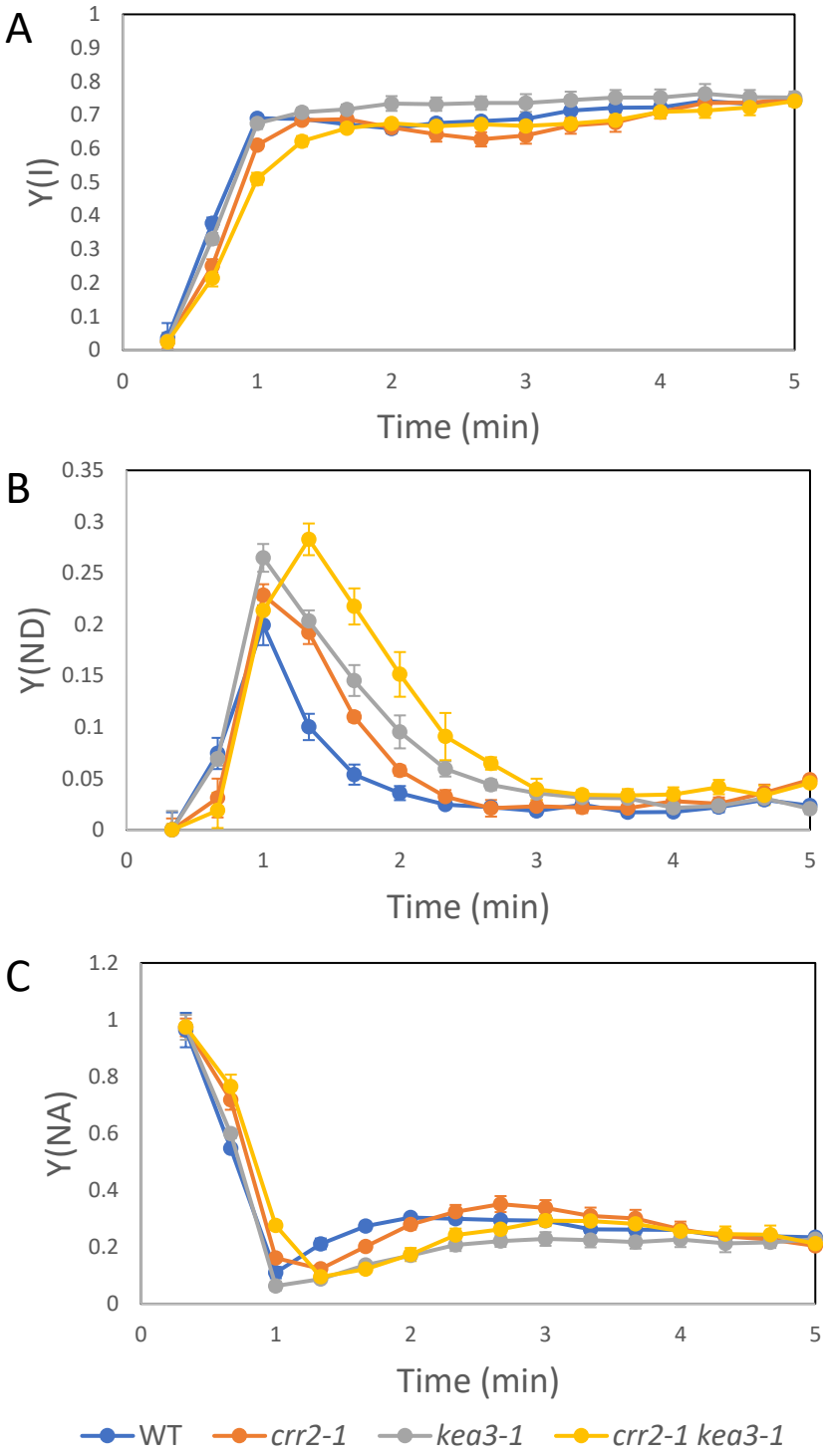

Figure 1-4. Induction of photosynthesis under non-saturating light (110 µmol photons m^{-2} s^{-1}) was monitored by P700 parameters after the 30-min dark adaptation. Yields of PSI, Y(I), (A), donor-side regulation of PSI, Y(ND) (B) and acceptor-side limitation of PSI, Y(NA) (C) were analyzed. A set of genotypes including *crr2-1* and *kea3-1* was analyzed. Data are shown as mean ± SE (n = 4–5). Detached leaves from dark-adapted plants were exposed to AL.

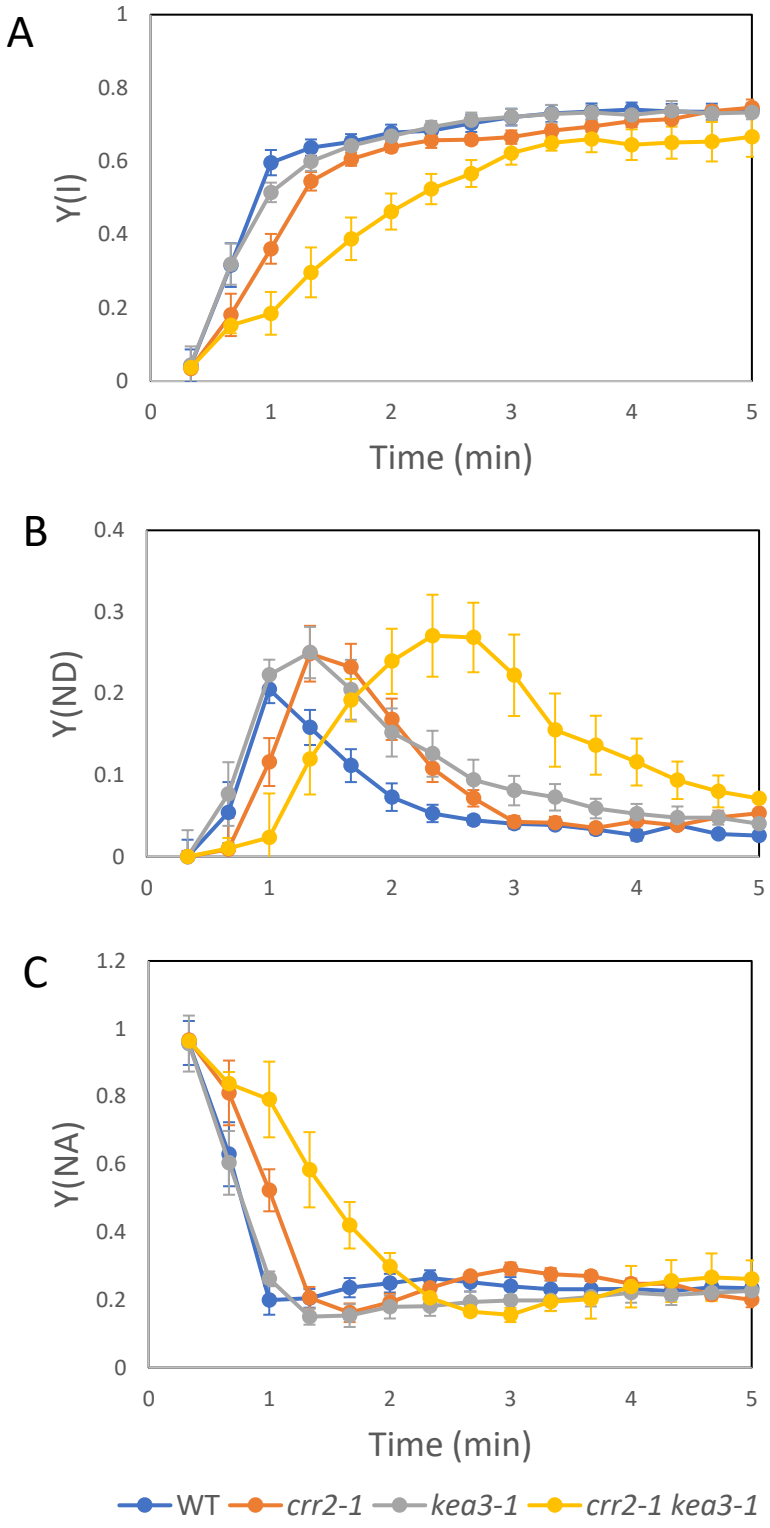

Figure 1-5. Induction of photosynthesis by non-saturating light (110 µmol photons m^{-2} s^{-1}) was monitored by P700 parameters after overnight dark adaptation. Yields of PSI, Y(I) (A), donor-side regulation of PSI, Y(ND) (B) and acceptor-side limitation of PSI, Y(NA) (C) were analyzed. Data are shown as mean ± SE (n = 4–5). Detached leaves from dark-adapted plants were exposed to AL. Triangles indicate the time points for statistical analyses summarized in Table 4.

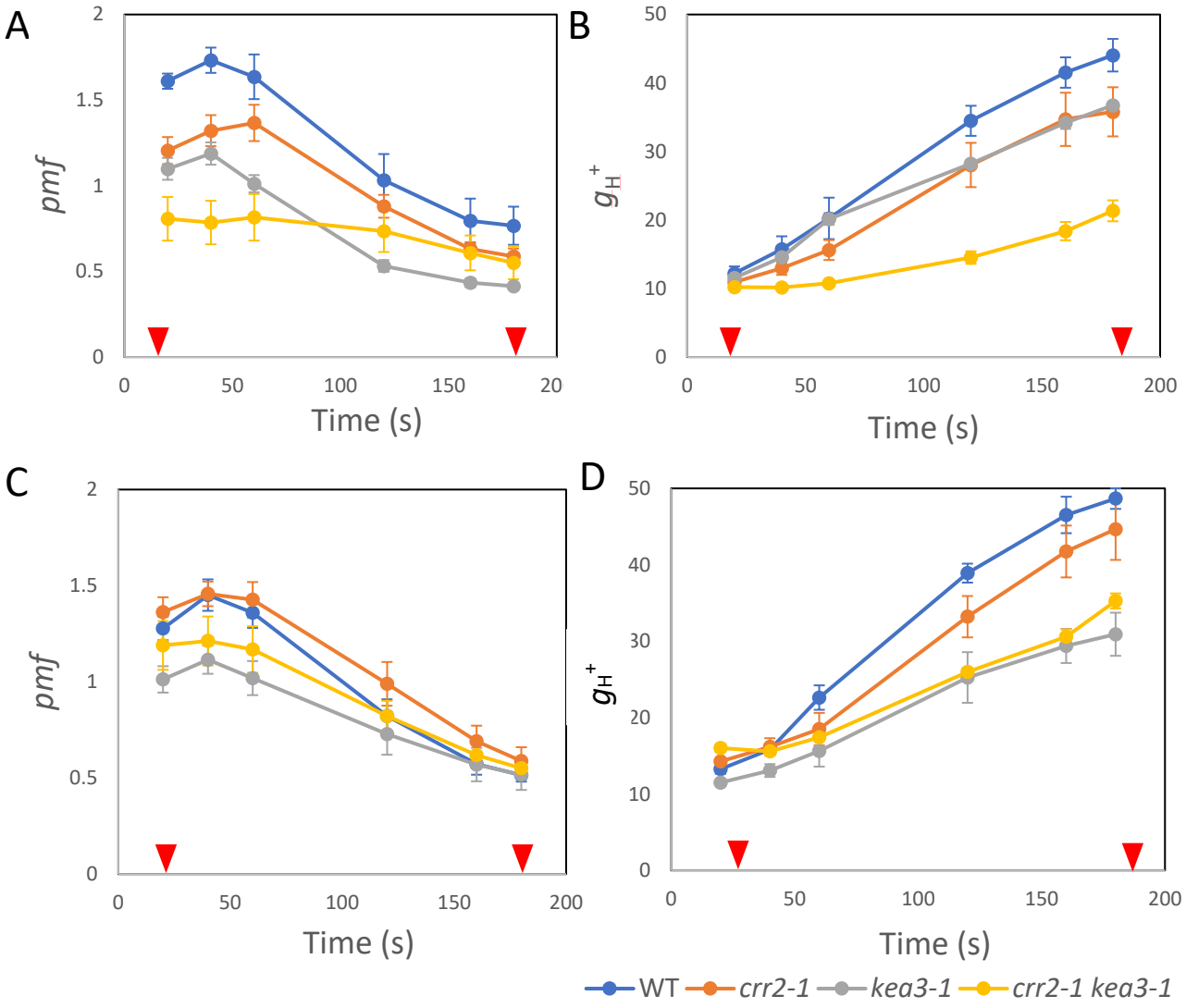

Figure 1-6. ECS analysis of a set of genotypes including *crr2-1* and *kea3-1*. Photosynthesis was induced by non-saturating light (110 µmol photons m^{-2} s^{-1}) after overnight dark adaptation (A and B) and 30-min dark adaptation (C and D). The size of light-induced pmf ($ECSt/ESC_{ST}$) (A and C) and proton conductivity of the thylakoid membrane (g_H^+) were determined. Data are shown as mean ± SE (n = 4–5). Detached leaves from dark-adapted plants were exposed to AL. Triangles indicate the time points for statistical analyses summarized in Table 5.

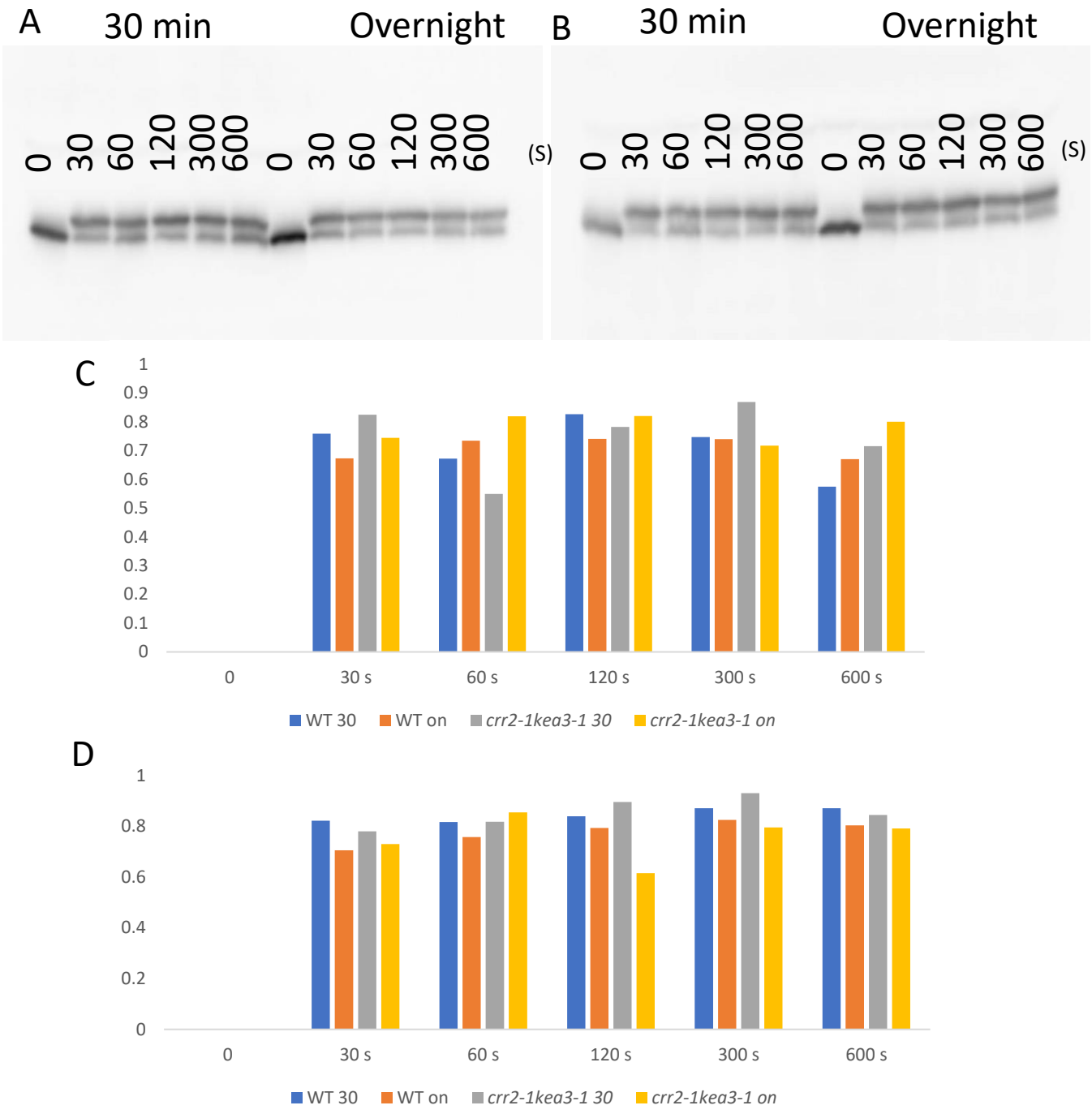

Figure 1-7. Photo-reduction patterns of the γ subunit of ATP synthase. Plants were placed under non-saturating light (110 μmol photons m^{-2} s^{-1}) for the indicated periods. Before the induction of photosynthesis, WT and *crr2-1 kea3-1* mutant plants were dark-adapted for overnight (on) and 30 min. (A) A representative blotting images. (B and C) Quantification of signal intensity in two independent experiments (biological replicates). The y-axis indicates the ratio of the reduced form of the γ subunit.

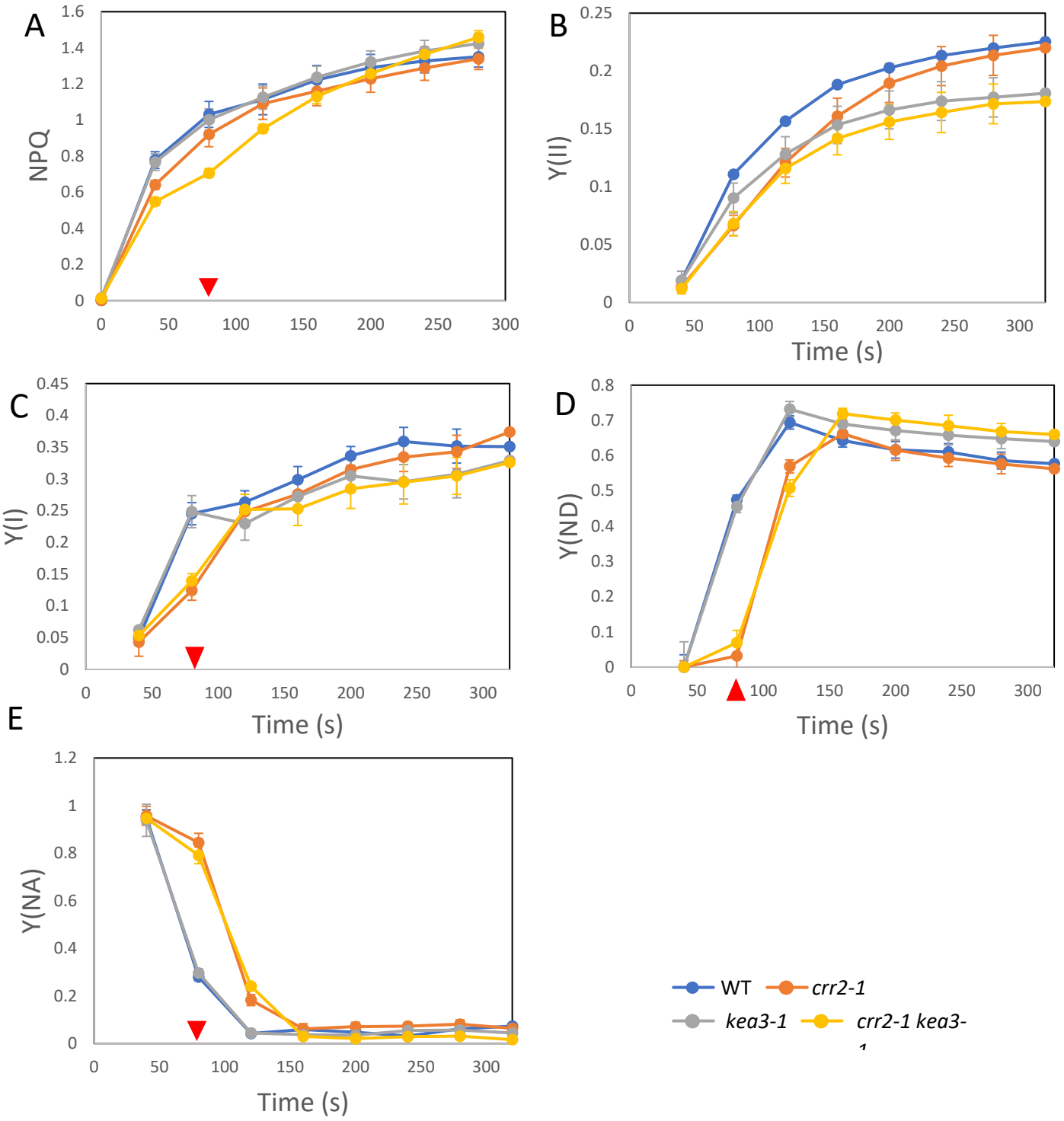

Figure 1-8. Induction of photosynthesis by relatively HL (300 µmol photons m^{-2} s^{-1}) after overnight dark adaptation. Induction and relaxation of NPQ (A) and induction of Y(II) (B) were measured by chlorophyll fluorescence in a set of genotypes including *crr2-1* and *kea3-1*. Yields of PSI, Y(I) (C), donor-side regulation of PSI, Y(ND) (D) and acceptor-side limitation of PSI, Y(NA) (E) were also analyzed by monitoring the P700 absorbance changes. Data are shown as mean ± SE (n = 5). Detached leaves from dark-adapted plants were exposed to AL. Triangles indicate the time points for statistical analyses summarized in Table 6.

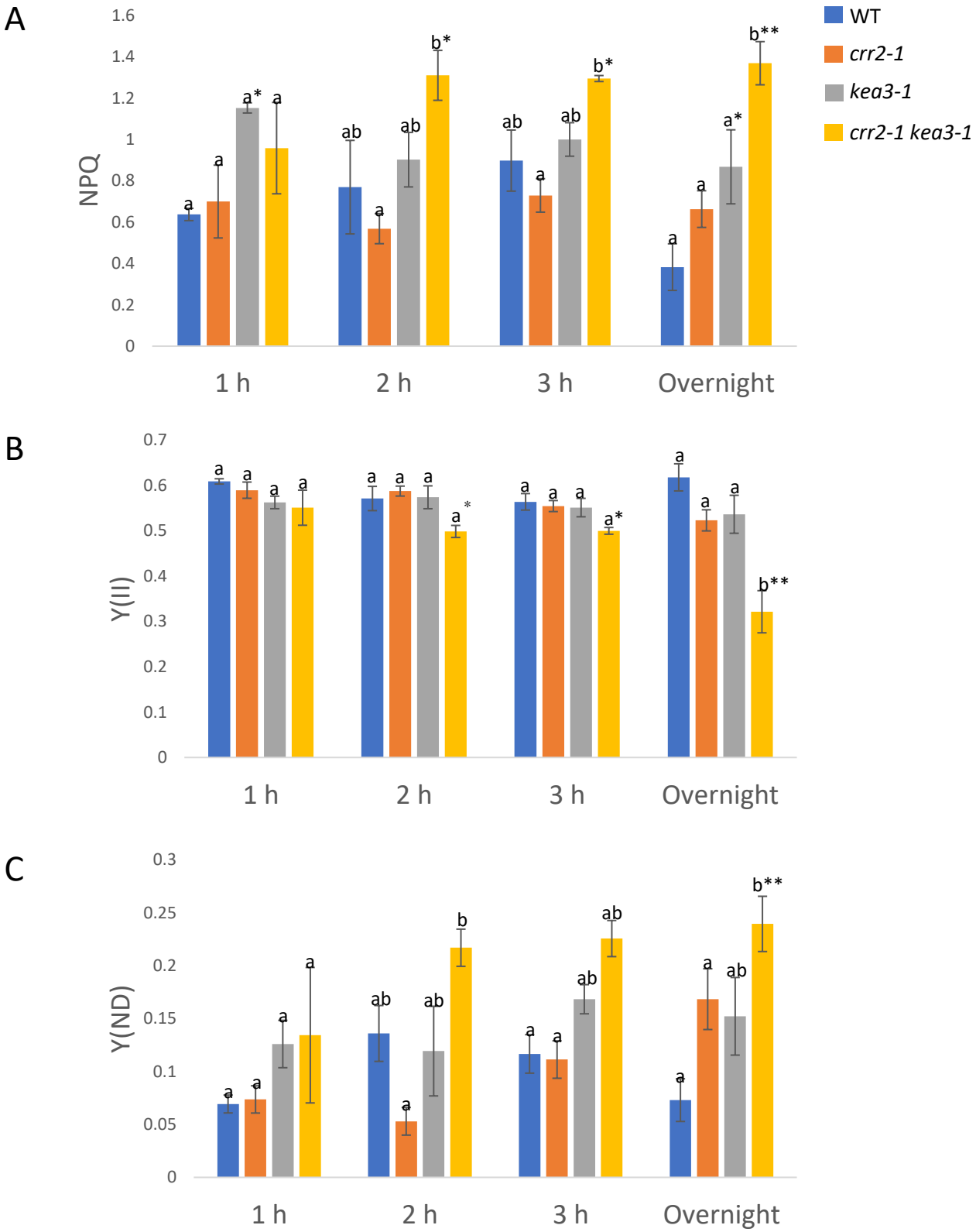

Figure 1-9. Impact of the time of dark adaptation on electron transport. Levels of NPQ (A), Y(II) (B) and Y(ND) (C) were determined at 3 min after the onset of AL after dark adaptation as described below graphs. Data are shown as mean ± SE (n = 3–5). Detached leaves from dark-adapted plants were exposed to AL. Different letters indicate the statistical differences confirmed by the Tukey-Kramer test ($P < 0.05$).

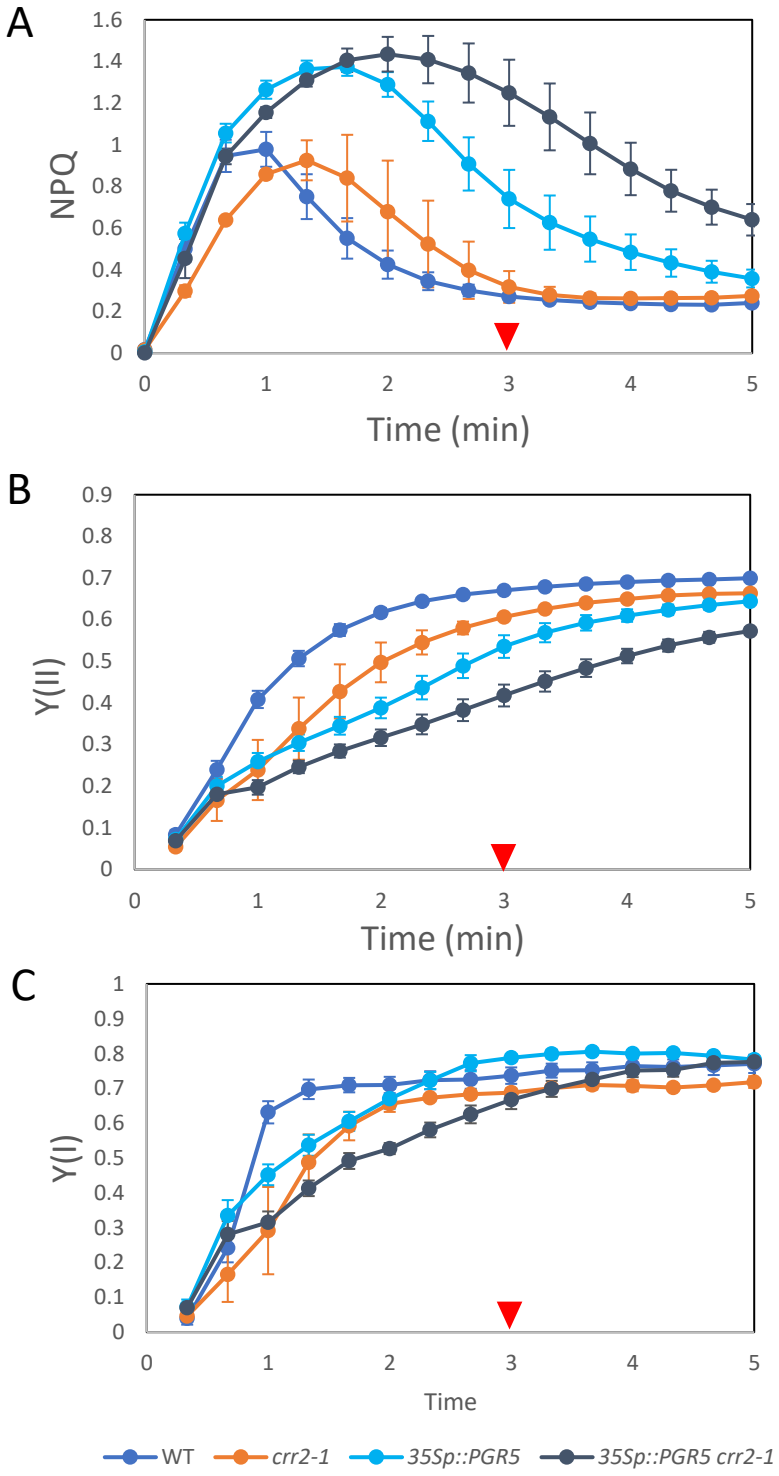

Figure 1-10. Induction of photosynthesis by non-saturating light (110 µmol photons m^{-2} s^{-1}) after overnight dark adaptation *crr2-1* and *35Sp::PGR5* was analyzed. Induction and relaxation of NPQ (A) and induction of Y(II) (B) and Y(I) (C) were measured by chlorophyll fluorescence (A and B) and P700 absorbance change (C) analyses. Data are shown as mean ± SE (n = 4–5). Detached leaves from dark-adapted plants were exposed to AL. Triangles indicate the time points for statistical analyses summarized in Table 7.

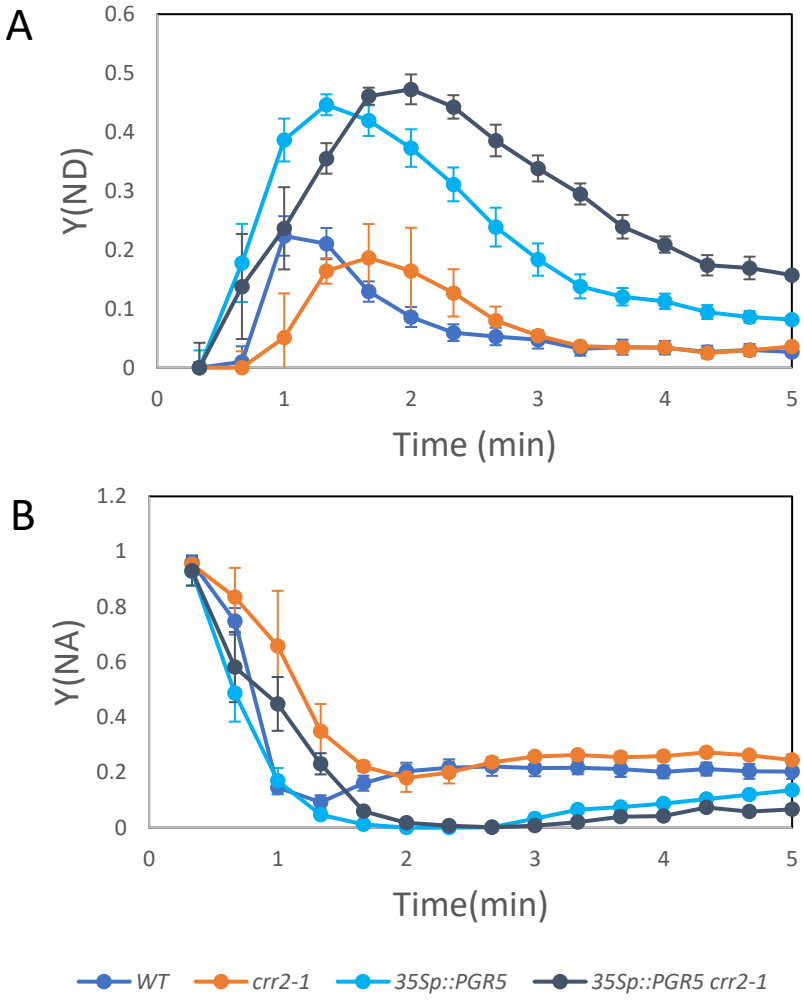

Figure 1-11. Induction of photosynthesis by non-saturating light (110 µmol photons m^{-2} s^{-1}) was monitored by P700 parameters after overnight dark adaptation. Donor-side regulation of PSI, Y(ND) (A) and acceptor-side limitation of PSI, Y(NA) (C) were analyzed. Data were from the same analysis as in Figure 5C. Data are shown as mean ± SD (n = 4–5). A set of genotypes including *crr2-1* and *35Sp::PGR5* was analyzed. Detached leaves from dark-adapted plants were exposed to AL. Triangles indicate the time point (3 min) for statistical analyses summarized in Table 7.

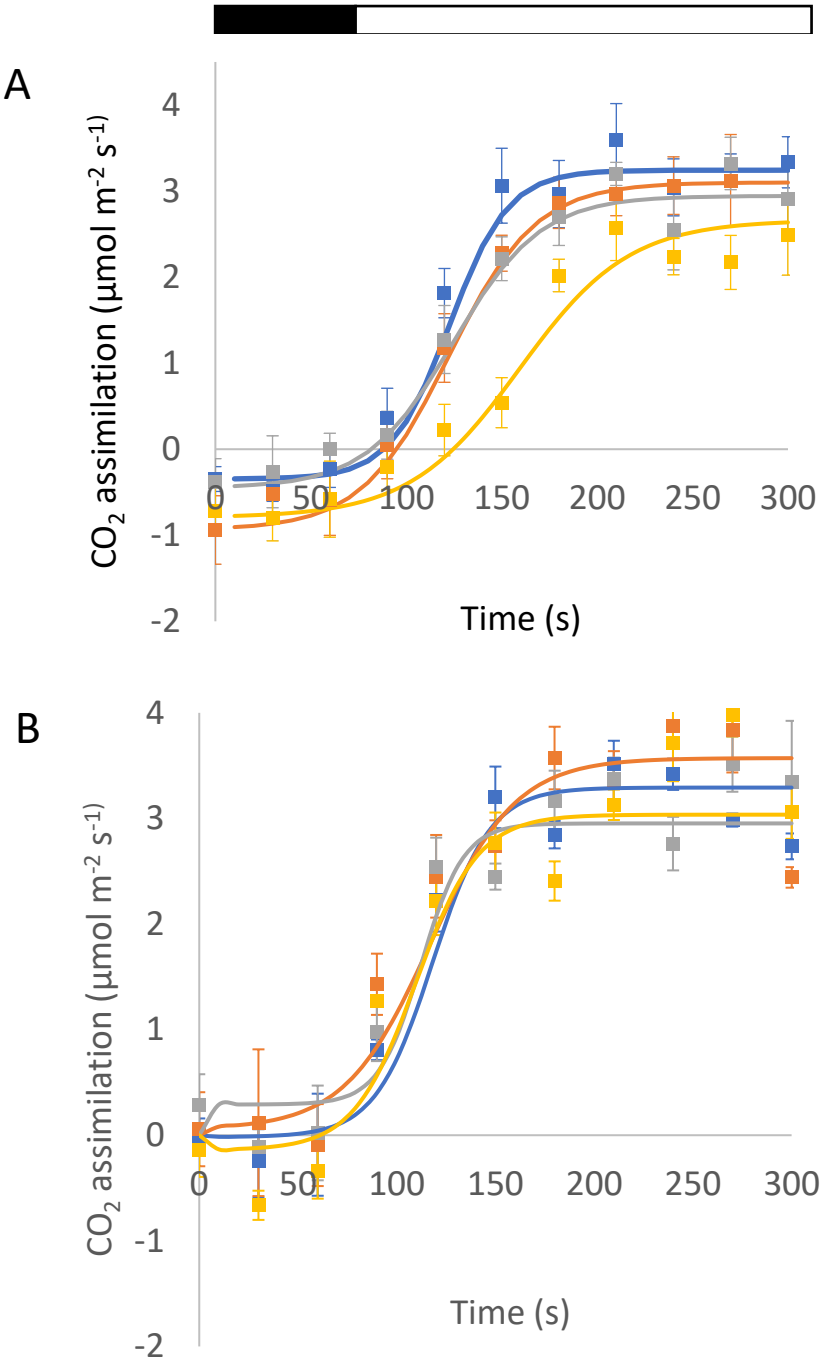

Figure 1-12. Analysis of CO_2 fixation under non-saturating light (110 µmol photons m^{-2} s^{-1}). A set of genotypes including *crr2-1*and *kea3-1* was analyzed. Data are shown as mean ± SE (*n* = 4–5). Detached leaves from dark-adapted plants were exposed to AL. The statistical analyses are summarized in Supplemental Fig. S8. The black and white bars represent the analysis in the dark and in the light, respectively.

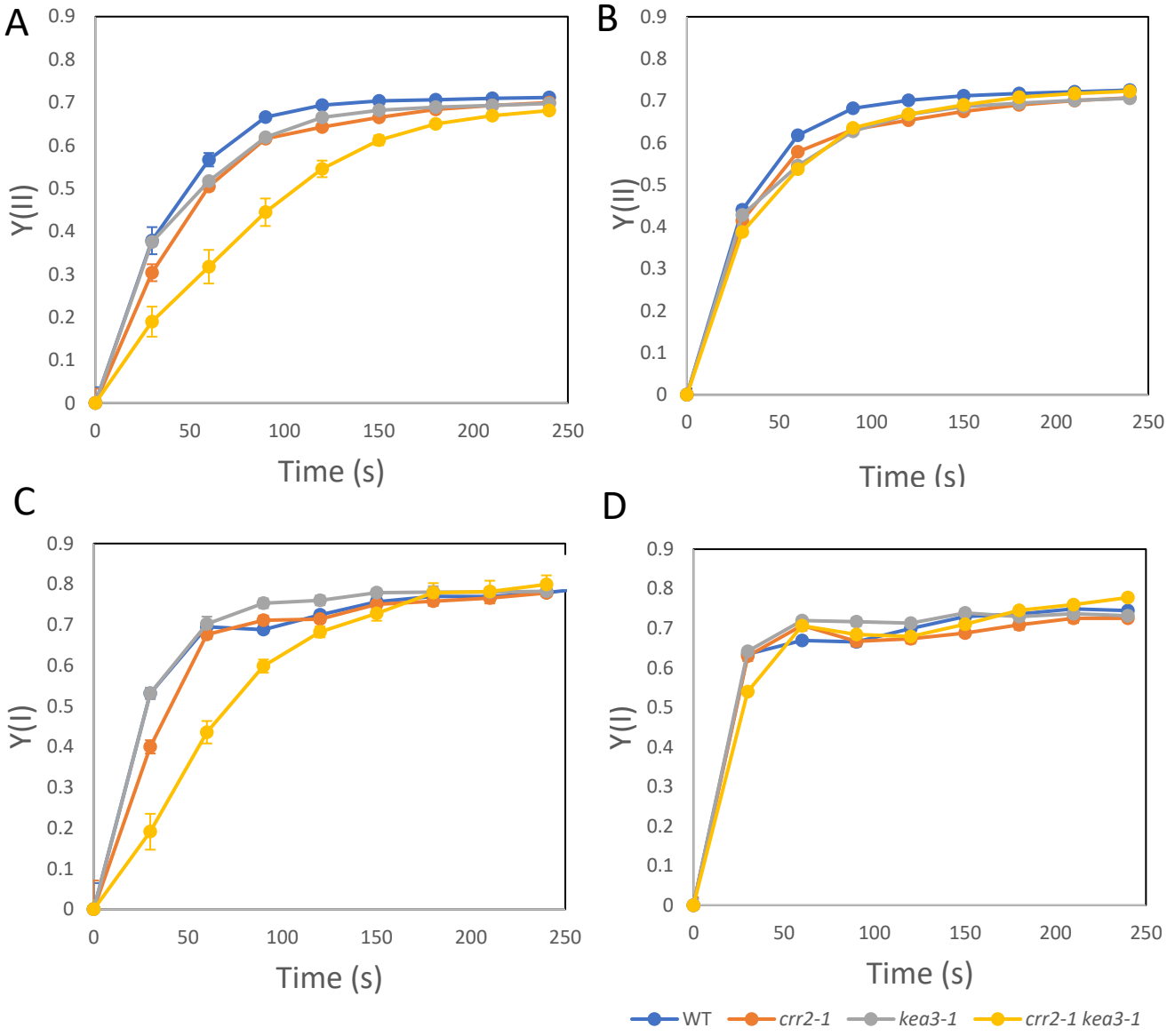

Figure 1-13. Chlorophyll fluorescence and P700 absorbance changes were simultaneously analyzed during the induction of CO_2 fixation (Fig. 7). Y(II) (A and B) and Y(I) (C and D) were determined after overnight (A and C) and 30-min (B and D) dark adaptation. The analysis was performed was simultaneously analyzed by Y(I) (B and E) and Y(II) (C and F) after overnight (A–C) and 30-min (D–F) dark adaptation. The statistical analyses are summarized in Table 8.

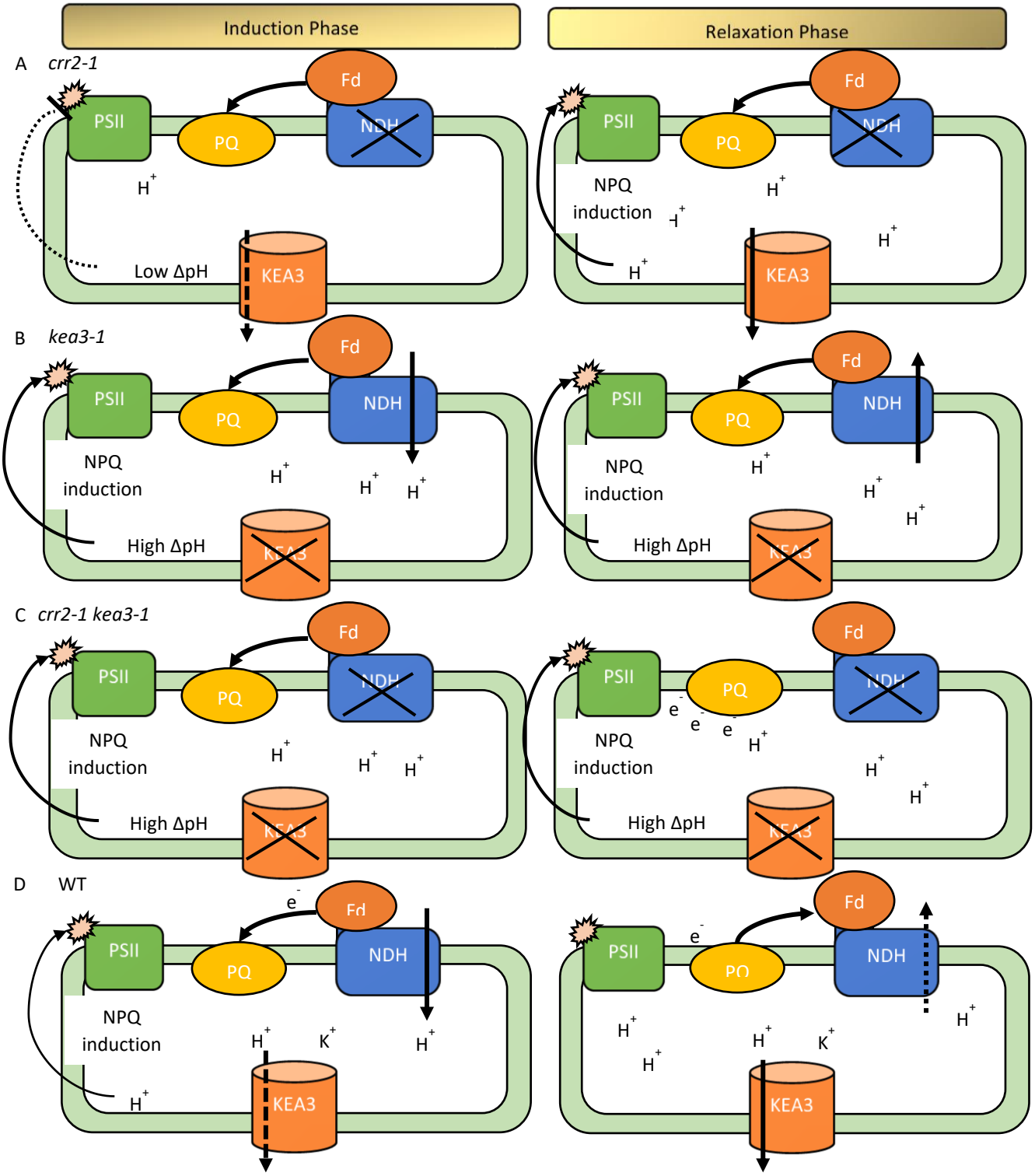

Figure 1-14: Schematic model of the regulation of photosynthetic induction by the collaboration of NDH and KEA3. Arrows indicate movement of protons. KEA3 is inactivated in the early phase (0-60 s). In *crr2-1*(A), the lack of NDH-dependent CET delays the induction of transient NPQ. In *kea3-1* (B), the KEA3-dependent relaxation of large ΔpH was inhibited. The reverse reaction of NDH partially alleviates this defect. In the *crr2-1 kea3-1* double mutant, induction of LET in the early phase (0-60 s) is severely delayed. It is unclear how KEA3 functions in this phase. In the subsequent phase (60-300 s) accumulation of protons in the thylakoid lumen drastically delays the induction of LET. In the WT (D) collaboration of KEA3 and NDH optimizes the induction of photosynthesis.

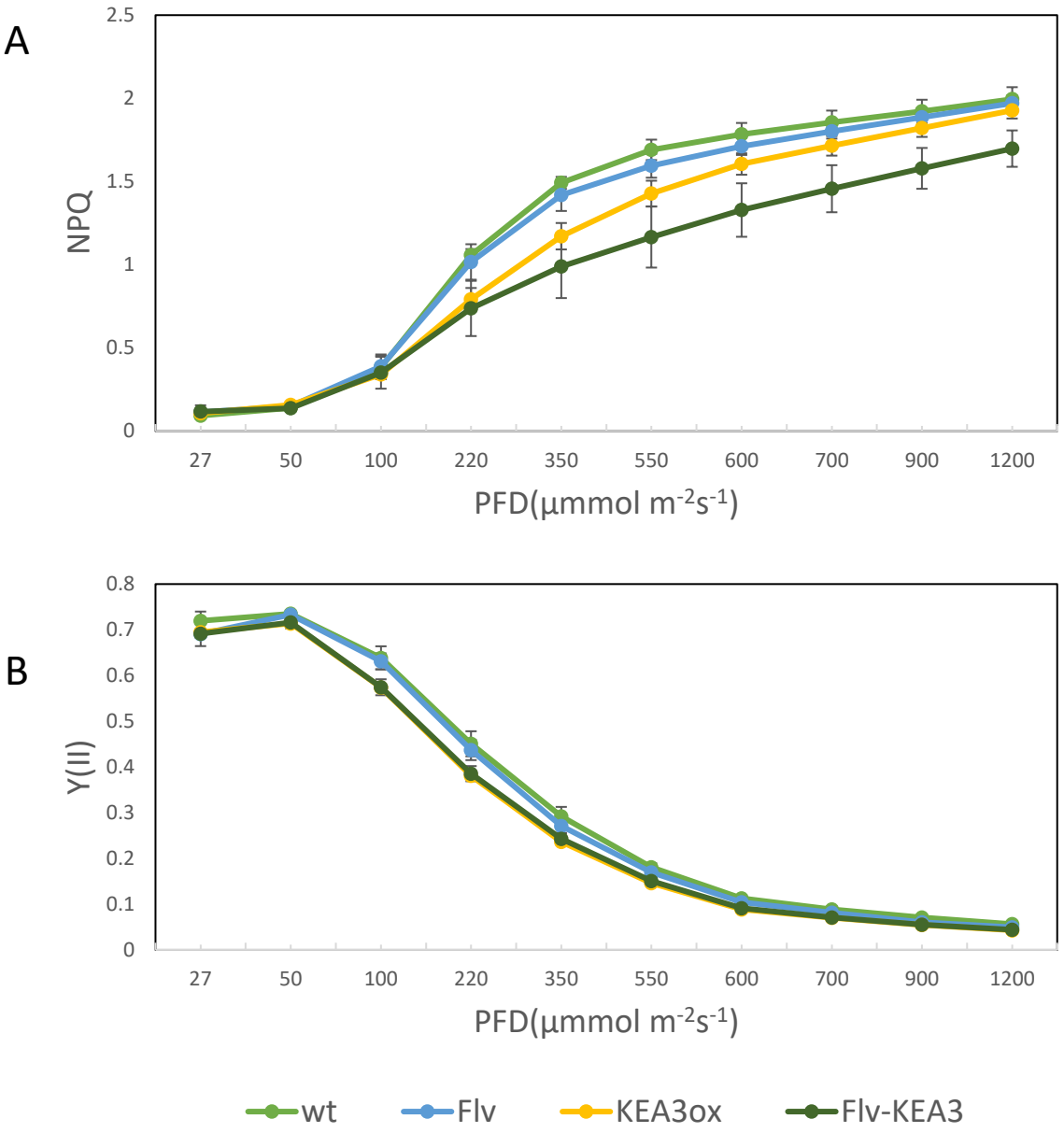

Figure 2-1. Impact of the overexpression of WT KEA3 and Flv on steady-state photosynthesis. The light intensity-dependence of chlorophyll fluorescence parameters, NPQ (A) and Y(II) (B), were determined in detached leaves of WT, Flv, KEA3ox, and Flv-KEA3 plants. Data represent means of 4 plants with SD. PFD, photon flux density.

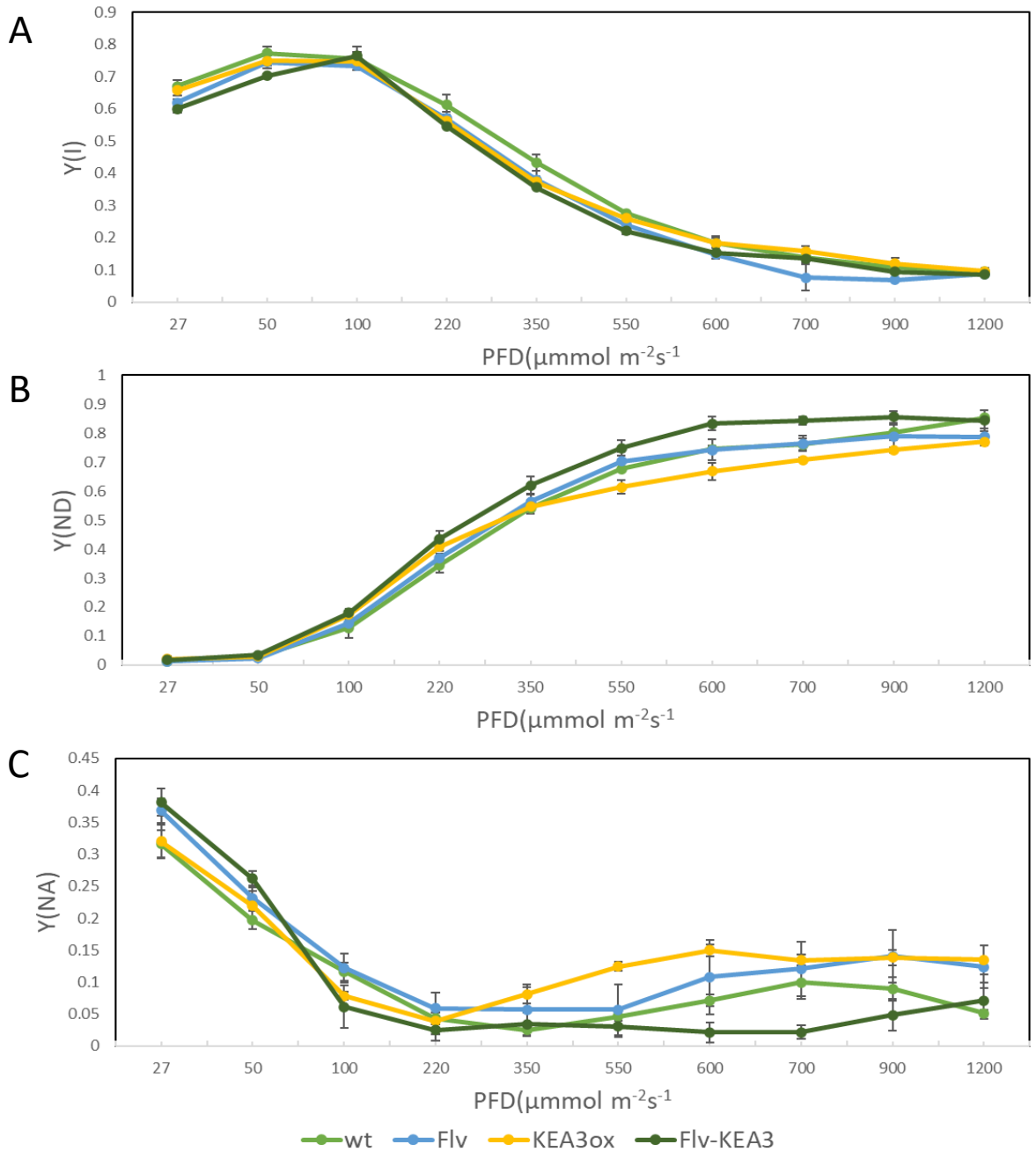

Figure 2-2. Impact of the overexpression of Flv and KEA3 on steady-state photosynthesis. The light intensity-dependence of P700 parameters, Y(I) (A), Y(ND) (B) and Y(NA) (C) were determined in detached leaves from WT, Flv, KEA3ox, and Flv-KEA3 plants. Data represent means of 4 plants with SD. PFD, photon flux density.

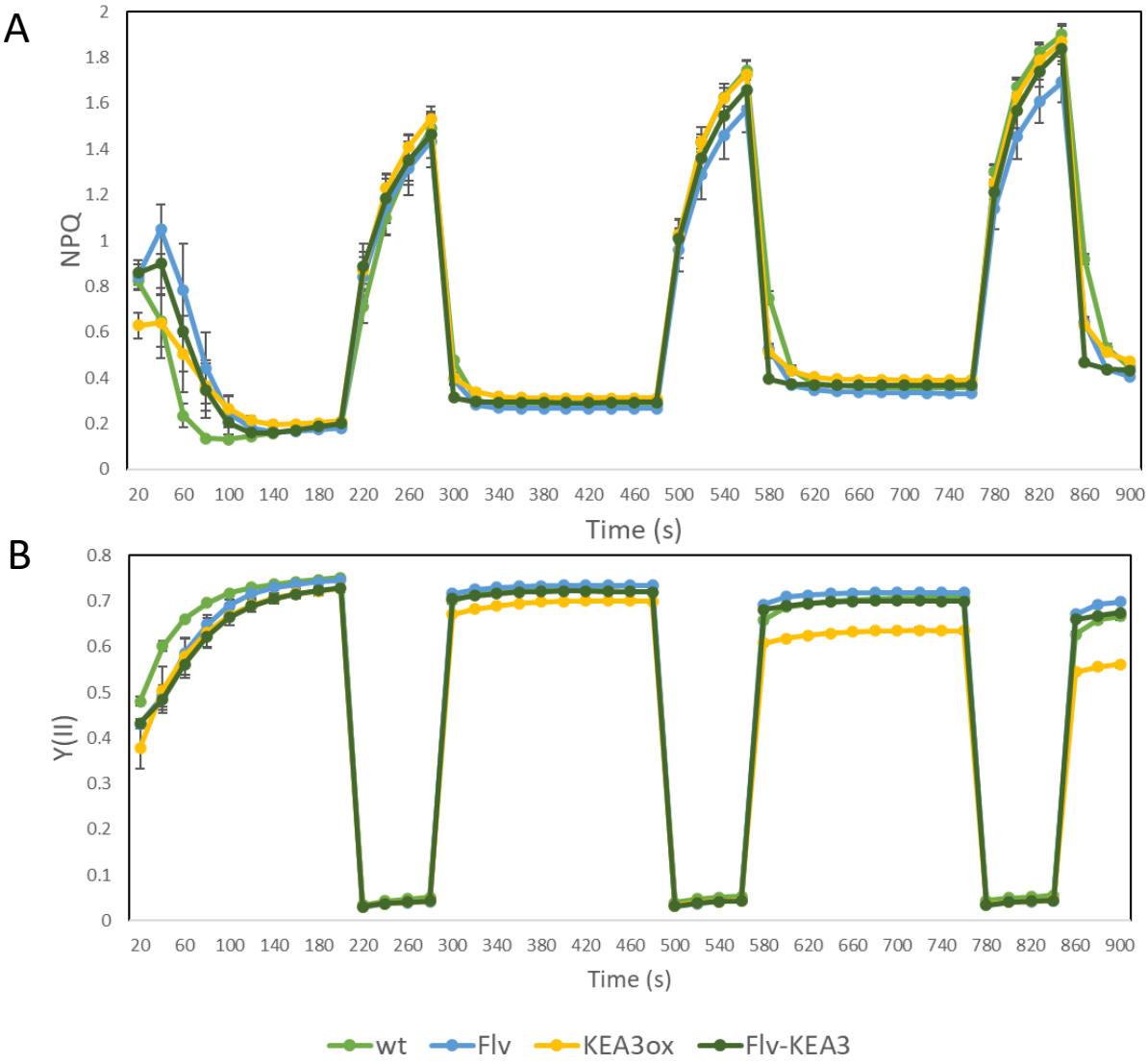

Figure 2-3. Effects of fluctuating light on photosynthetic parameters determined by Dual-PAM in detached leaves from WT, Flv, KEA3ox, and Flv-KEA3 plants. Chlorophyll fluorescence parameters are NPQ (A) and Y(II) (B). Detached leaves from plants dark adapted for 30 min (black bar) were exposed to three cycles of fluctuating light. Each cycle consisted of 4 min of LL (47 mmol photons m-2 s-1) followed by 1 min of HL (1,529 mmol photons m-2 s-1). Data represent means of 4 plants with SD.

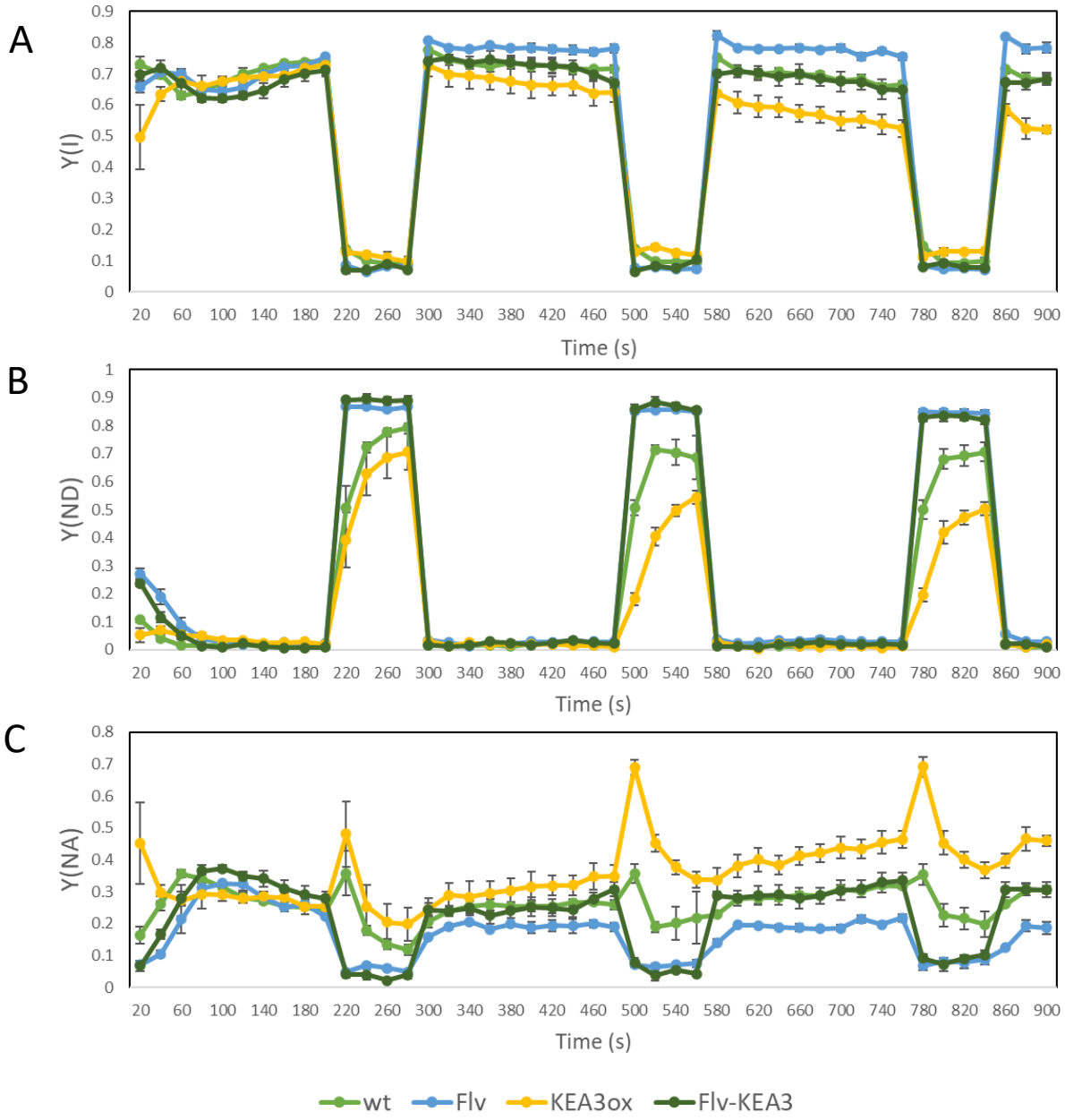

Figure 2-4. Effects of fluctuating light on photosynthetic parameters determined by Dual-PAM in detached leaves from WT, Flv, KEA3ox, and Flv-KEA3 plants. Parameters were Y(I) (A), Y(ND) (B) and Y(NA) (C). Detached leaves from plants dark adapted for 30 min (black bar) were exposed to three cycles of fluctuating light. Each cycle consisted of 4 min of LL (47 mmol photons m-2 s-1) followed by 1 min of HL (1,529 mmol photons m-2 s-1). Data represent means of 4 plants with SD.